AMERICAN SOCIETY FOR MICROBIOLOGY | Applied and Environmental Microbiology®

ENVIRONMENTAL MICROBIOLOGY

Thermophilic Carboxylesterases from Hydrothermal Vents of the Volcanic Island of Ischia Active on Synthetic and Biobased Polymers and Mycotoxins

Marco A. Distaso,[a] Tatyana N. Chernikova,[a] Rafael Bargiela,[a] Cristina Coscolín,[b] Peter Stogios,[c] Jose L. Gonzalez-Alfonso,[b] Sofia Lemak,[c] Anna N. Khusnutdinova,[a] Francisco J. Plou,[b] Elena Evdokimova,[c] Alexei Savchenko,[c,d] Evgenii A. Lunev,[a,e] Michail M. Yakimov,[f] Olga V. Golyshina,[a] Manuel Ferrer,[b] Alexander F. Yakunin,[a,c] Peter N. Golyshin[a]

[a]Centre for Environmental Biotechnology, School of Natural Sciences, Bangor University, Bangor, United Kingdom
[b]Department of Applied Biocatalysis, ICP, CSIC, Madrid, Spain
[c]Department of Chemical Engineering and Applied Chemistry, University of Toronto, Toronto, Canada
[d]Department of Microbiology Immunology and Infectious Diseases, University of Calgary, Calgary, Canada
[e]Institute of Gene Biology, Russian Academy of Sciences, Moscow, Russia
[f]Institute of Polar Sciences, National Research Council, Messina, Italy

Manuel Ferrer, Alexander F. Yakunin, and Peter N. Golyshin contributed equally to this work.

ABSTRACT Hydrothermal vents are geographically widespread and host microorganisms with robust enzymes useful in various industrial applications. We examined microbial communities and carboxylesterases of two terrestrial hydrothermal vents of the volcanic island of Ischia (Italy) predominantly composed of *Firmicutes*, *Proteobacteria*, and *Bacteroidota*. High-temperature enrichment cultures with the polyester plastics polyhydroxybutyrate and polylactic acid (PLA) resulted in an increase of *Thermus* and *Geobacillus* species and to some extent *Fontimonas* and *Schleiferia* species. The screening at 37 to 70°C of metagenomic fosmid libraries from above enrichment cultures identified three hydrolases (IS10, IS11, and IS12), all derived from yet-uncultured *Chloroflexota* and showing low sequence identity (33 to 56%) to characterized enzymes. Enzymes expressed in *Escherichia coli* exhibited maximal esterase activity at 70 to 90°C, with IS11 showing the highest thermostability (90% activity after 20-min incubation at 80°C). IS10 and IS12 were highly substrate promiscuous and hydrolyzed all 51 monoester substrates tested. Enzymes were active with PLA, polyethylene terephthalate model substrate, and mycotoxin T-2 (IS12). IS10 and IS12 had a classical α/β-hydrolase core domain with a serine hydrolase catalytic triad (Ser155, His280, and Asp250) in their hydrophobic active sites. The crystal structure of IS11 resolved at 2.92 Å revealed the presence of a N-terminal β-lactamase-like domain and C-terminal lipocalin domain. The catalytic cleft of IS11 included catalytic Ser68, Lys71, Tyr160, and Asn162, whereas the lipocalin domain enclosed the catalytic cleft like a lid and contributed to substrate binding. Our study identified novel thermotolerant carboxylesterases with a broad substrate range, including polyesters and mycotoxins, for potential applications in biotechnology.

IMPORTANCE High-temperature-active microbial enzymes are important biocatalysts for many industrial applications, including recycling of synthetic and biobased polyesters increasingly used in textiles, fibers, coatings and adhesives. Here, we identified three novel thermotolerant carboxylesterases (IS10, IS11, and IS12) from high-temperature enrichment cultures from Ischia hydrothermal vents and incubated with biobased polymers. The identified metagenomic enzymes originated from uncultured *Chloroflexota* and showed low sequence similarity to known carboxylesterases. Active sites of IS10 and IS12 had the largest effective volumes among the characterized prokaryotic carboxylesterases and exhibited high substrate promiscuity, including hydrolysis of polyesters and mycotoxin T-2 (IS12). Though less promiscuous than IS10 and IS12, IS11 had a higher thermostability with a high temperature optimum (80 to 90°C) for activity and hydrolyzed polyesters, and its

Editor Haruyuki Atomi, Kyoto Daigakul

Address correspondence to Manuel Ferrer, mferrer@icp.csic.es, or Peter N. Golyshin, p.golyshin@bangor.ac.uk.

The authors declare no conflict of interest.

Received 3 October 2022
Accepted 29 December 2022
Published 31 January 2023

crystal structure revealed an unusual lipocalin domain likely involved in substrate binding. The polyesterase activity of these enzymes makes them attractive candidates for further optimization and potential application in plastics recycling.

KEYWORDS thermophilic bacteria, hydrothermal vents, Ischia, metagenome screening, carboxylesterase, polyesterase, 3PET, PLA, biochemical characterization, crystal structure

Environmental microbial communities and microorganisms represent an enormous reserve of biochemical diversity and enzymes for fundamental research and applications in biotechnology (1, 2). However, the vast majority of environmental microbes have never been grown and characterized in the laboratory (3, 4). The metagenomic approach has emerged as a strategic way to study unculturable microorganisms and their enzymes by using various computational and experimental methods (5–7). Metagenomics includes shotgun sequencing of microbial DNA purified from a selected environment, high-throughput screening of metagenomic expression libraries (functional metagenomics), profiling of RNAs and proteins produced by a microbial community (metatranscriptomics and metaproteomics), and identification of metabolites and metabolic networks of a microbial community (metametabolomics) (8). Global DNA sequencing efforts and several large-scale metagenome sampling projects revealed the vast sequence diversity in environmental metagenomes and microbial genomes, as well as the presence of numerous unknown or poorly characterized genes (9–12). For example, a high-throughput project focused on carbohydrate-active enzymes identified over 27,000 related genes and demonstrated the presence of glycoside hydrolase activity in 51 of 90 tested proteins (13). Other large-scale metagenomic projects include the Sargasso Sea sampling (over 1 million new genes discovered), the Global Ocean Survey (over 6 million genes), and human gut microbiome (over 3 million genes) (9–12). Thus, through the advent of metagenomics, we are starting to generate insights into the rich microbial worlds thriving in different environments. Nevertheless, a recent analysis of metagenome screening studies suggested that all representative types of environmental habitats (terrestrial, marine, and freshwater) are undersampled and underinvestigated (14). It is estimated that the total number of microbial cells is 10^{30}, whereas the natural protein universe exceeds 10^{12} proteins, indicating that our knowledge of proteins and biochemical diversity on Earth is very limited (15–17). Therefore, the determination of protein function or enzyme activity for millions of genes of unknown function and biochemically uncharacterized proteins represents one of the main challenges of postgenomic biology.

The approaches of experimental metagenomics include metatranscriptomics, metaproteomics, metabolomics, and enzyme screening (6, 7, 17–19). Activity-based screening of metagenome gene libraries represents a direct way for tapping into the metagenomic resource of novel enzymes. This approach involves expressing genes from metagenomic DNA fragments in heterologous hosts, commonly *Escherichia coli*, and assaying libraries of clones on agar plates for enzymatic activities using chromogenic or insoluble substrates (18). Importantly, this approach offers the possibility to identify novel families of enzymes with no sequence similarity to known enzymes. Screening of metagenome gene libraries from different terrestrial, marine, and freshwater environments has already expanded the number of new enzymes, including novel nitrilases, glycoside hydrolases, carboxyl esterases, and laccases (14, 20, 21).

Carboxylesterases (EC 3.1.1.1) are a diverse group of hydrolytic enzymes catalyzing the cleavage and formation of ester bonds and represent the third largest group of industrial biocatalysts (after amylases and proteases). Many esterases show a wide substrate range and high regio- and stereoselectivity, making them attractive biocatalysts for applications in pharmaceutical, cosmetic, detergent, food, textile, paper, and biodiesel industries (22, 23). Most of known carboxylesterases belong to the large protein superfamilies of α/β-hydrolases and β-lactamases and have been classified into 46 subfamilies (including 11 true lipase subfamilies) based on sequence analysis (22, 24, 25). A significant number of these enzymes have been characterized both biochemically and structurally, because they

are of high interest for biotechnological applications (22, 23, 26). Screening of metagenome gene libraries and genome mining have greatly expanded the number of novel carboxylesterases, including enzymes active against aryl esters or polymeric esters (polyesterases) (21–23, 26, 27). However, the increasing demand for environmentally friendly industrial processes has stimulated research on the discovery of new enzymes and their application as biocatalysts to meet the challenges of a circular bioeconomy (28, 29). The global enzyme market is expected to grow from $8.18 billion in 2015 to $17.50 billion by 2024 (28). However, the majority of known enzymes originated from mesophilic organisms, which have limited stability under harsh industrial conditions, including high temperatures, extreme pH, solvents, and salts (30, 31). Thus, the discovery of robust enzymes, including carboxylesterases, and engineering of more active variants represent the key challenges for the development of future biocatalytic processes. Extremophilic microorganisms are an attractive source of industrial biocatalysts, because they evolved robust enzymes that function under extreme conditions (high or low temperatures, high or low pH, salts) (14, 26, 30, 32). In addition, extremophilic enzymes found in one environment are typically also tolerant to other extreme conditions, making them attractive biocatalysts for various applications, including depolymerization of synthetic polymers and inactivation of mycotoxins (32–36).

Hydrothermal vents are extreme environments located in tectonically active sites, which are classified as terrestrial and marine (deep sea and shallow sea) systems (37). Hydrothermal vents are characterized by harsh physicochemical conditions (high temperature and low pH) and are known as sources of thermophilic microbes and enzymes with biotechnological importance. Although terrestrial hydrothermal vents have relatively easy access, they remain underinvestigated compared to (sub)marine hydrothermal vents. To provide insights into microbial diversity of terrestrial hydrothermal vents, we analyzed the natural microbial communities of two thermophilic hydrothermal vents located on the volcanic island of Ischia (Italy), as well as the effect of polyester plastic addition on these microbial communities, by using barcoded DNA sequencing of extracted DNA. Using an activity-based metagenomic approach, we screened fosmid libraries for carboxylesterase activity using tributyrin agar plates, and we identified 14 unique fosmids encoding putative hydrolases, from which three soluble carboxylesterases (IS10, IS11, and IS12) were recombinantly produced in *E. coli* and biochemically characterized, including substrate range and stability, by using both monoester and polyester substrates. The crystal structure of IS11 was resolved to reveal an N-terminal β-lactamase-like serine hydrolase domain connected to the C-terminal lipocalin domain. The active site of IS11 accommodated the conserved catalytic residues Ser68, Lys71, Tyr160, and Asn162, as well as numerous hydrophobic residues potentially involved in substrate binding. Structural models of IS10 and IS12 revealed classical α/β-hydrolase domains with a catalytic serine hydrolase triad (Ser155, His280, and Asp250) and multiple hydrophobic residues in their active sites, with the largest effective volumes reported for prokaryotic carboxylesterases.

RESULTS AND DISCUSSION

Natural microbial communities of terrestrial hydrothermal vents of Ischia and effects of polyester enrichments. To provide insights into the composition of natural microbial communities and thermophilic enzymes of hydrothermal vents of the island of Ischia, four sediment samples were collected from the Cavascura hot spring (samples IS1 and IS2) and from Maronti Beach near Sant'Angelo (samples IS3 and IS4) (see Materials and Methods). Both sites represent thermophilic habitats with slightly different environmental conditions: IS1 (pH 7.0, 45°C), IS2 (pH 8.5, 55°C), IS3 (pH 4.5, 75°C), and IS4 (pH 5.0, 85°C) (see Table S1 in the supplemental material). From each sample, total DNA was extracted and subjected to barcoded amplicon sequencing of the V4 region of the 16S rRNA gene. Sequence analysis revealed that the IS1 community comprised mainly *Pseudomonas* (17.2%), class *Anaerolineae* (*Chloroflexi*) (12.3%), class *Armatimonadota* (10.0%), *Elizabethkingia* (phylum *Bacteroidota*) (9.5%), other *Myxococcota* (9.1%), *Sphingobacterium* (order *Sphingobacteriales*, class *Bacteroidia*, phylum *Bacteroidota*) (6.7%), and class *Nitrospirota* (6.4%), whereas the IS2 community was dominated by *Caldimonas* (order

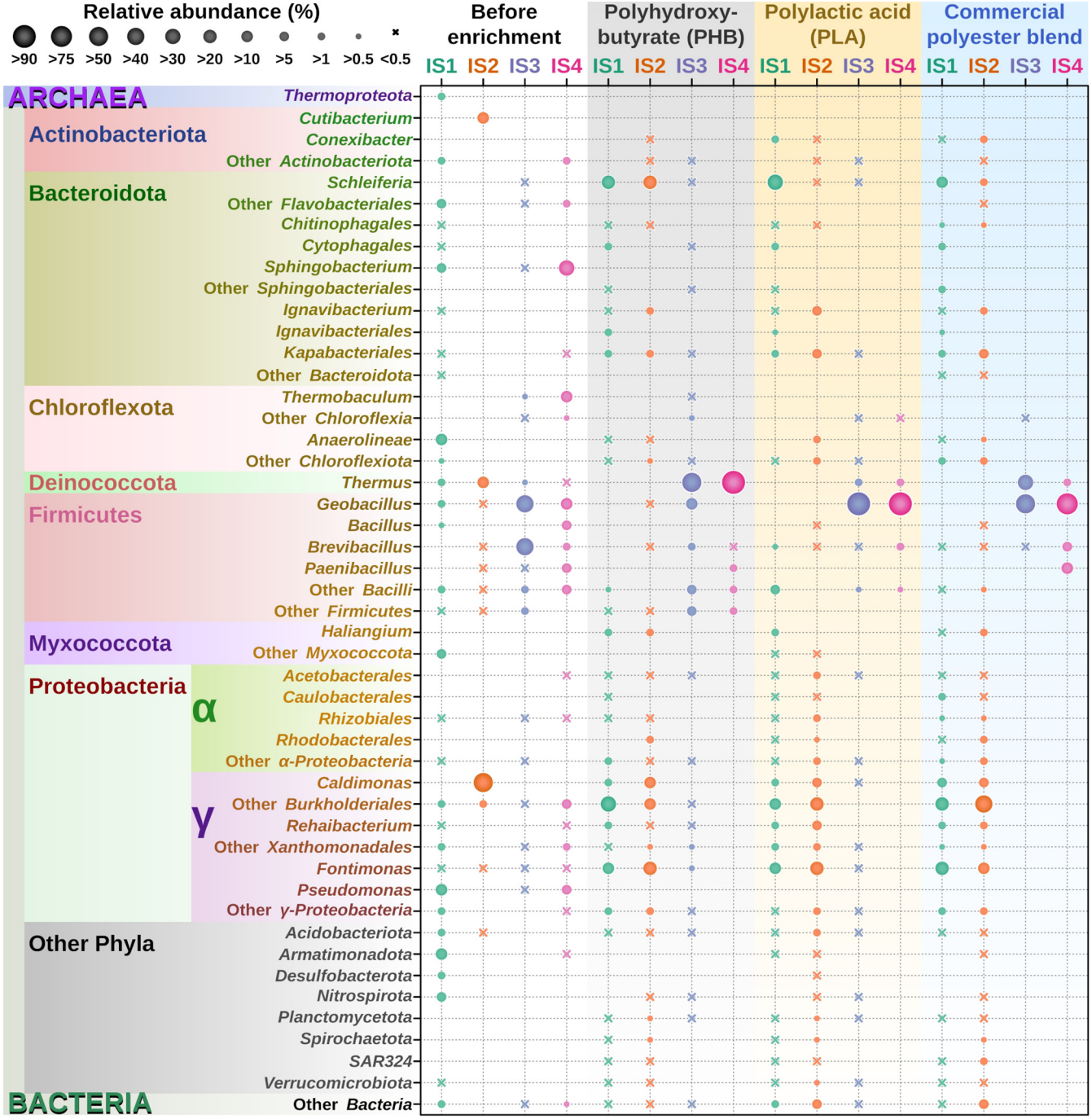

FIG 1 The composition of microbial communities of native samples from the Ischia hydrothermal vents (IS1 [green] and IS2 [orange], both from Cavascura, and IS3 [purple] and IS4 [magenta], both from Maronti Beach) and their enrichment cultures set up with PHB, PLA, and polyester blend and incubated for 4 days at 50°C (IS1 and IS2) or 75°C (IS3 and IS4), with consequent transfer into the fresh medium and incubation at the same temperatures for 11 days. The relative abundances of the barcoded V4 region 16S rRNA gene amplicon reads derived from particular taxa are reflected in the sizes of circles (for reference, see the scale in the top left corner).

Burkholderiales, class *Gammaproteobacteria*) (63.9%), *Cutibacterium* (order *Propionibacteriales*, class *Actinobacteria*) (17.2%), and *Thermus* (phylum *Deinococcota*) (16%) (Fig. 1). In contrast, the IS3 community was mainly represented by *Bacillales* (*Firmicutes*), namely, *Brevibacillus* (48.3%) and *Geobacillus* (42%), and other bacilli (4.4%), whereas IS4 comprised *Sphingobacterium* (*Sphingobacteriales*, *Bacteroidetes*) (31.9%), *Thermobaculum* (*Thermobaculales*, *Chloroflexi*) (17.4%), and *Geobacillus* (10.7%), followed by *Pseudomonas* (7%) and *Bacillus* (6.1%) (Fig. 1). The observed differences in the taxonomic compositions of the Cavascura (IS1 and IS2) and Maronti (IS3 and

IS4) samples can be attributed to different environmental conditions (temperature and pH) at the sampling sites.

Using the four sediment samples from the two Ischia sites, 12 enrichment cultures were established with different polyester plastics as carbon substrate, including polyhydroxybutyrate (PHB), polylactic acid (PLA), and commercial polyester blend (Table S1). After 2 weeks of incubation with polyesters, the IS1 enrichment culture showed a drastic increase in the relative abundance of members of the order *Burkholderiales* within the families *Comamonadaceae* and *Rhodocyclaceae* (relative abundance, 15.2 to 35.1% across the three plastic enrichments), *Fontimonas* (*Solimonadaceae*, 16.9 to 27.5%), and *Schleiferia* (order *Flavobacteriales*, 15.6 to 34.4%) (Fig. 1). Likewise, IS2 enrichment showed an increase in *Fontimonas* (11 to 26%) and *Schleiferia* (21% in PHB enrichment), whereas the relative content of *Caldimonas* decreased from 63% to 5.7%, in favor of members of other families of the order *Burkholderiales*, namely, *Rhodocyclaceae*, *Hydrogenophilaceae*, and *Comamonadaceae* (18 to 43%) *Kapabacteriales* (phylum *Bacteroidota*, 2.9 to 8%) and *Rehaibacterium* (order *Xanthomonadales*, 0.3 to 9.3%) (Fig. 1). The enrichment culture with the compostable P3 blend stimulated the growth of *Rhodocyclales*, as both IS1 and IS2 showed a strong increase in *Thauera* compared to experiments with PHB and PLA (Fig. 1). In the enrichment cultures IS3 and IS4, the higher incubation temperature (75°C) selected for thermophilic bacteria and the nature of polyester used for enrichments influenced the microbial composition (Fig. 1). The PHB enrichment stimulated growth of *Thermus* (*Deinococcota*), which accounted for 66.7% (92-fold increase) and 90.9% (1,280-fold increase) of the total reads in IS3 and IS4, respectively, followed by *Geobacillus* and other members of *Firmicutes*. In contrast, the PLA culture favored growth of *Geobacillus*, which reached a relative abundance of 95.8% in IS3 (2.3-fold increase) and 91.8% in IS4 (8.6-fold increase), followed by *Thermus* and *Brevibacillus*. Finally, the commercial polyester blend promoted growth of both *Geobacillus* (accounting for 68%, or 1.6-fold increase) and *Thermus* (accounting for 31.5%, or 43.8-fold increase) in the IS3 enrichment, whereas the IS4 culture was dominated by *Firmicutes*, *Geobacillus* (81%), *Paenibacillus* (11.9%), *Brevibacillus* (5.9%), and *Thermus* (1.18%). As expected, the Shannon index of microbial diversity (a measure of diversity of species in a community) (Fig. S1) revealed an overall tendency to decrease after incubation with polyester plastics, with the exception of IS2, which also showed low diversity in the native sample with the flattened rarefaction curve (Fig. S1).

Activity-based screening of the hydrothermal metagenome library from Ischia for carboxylesterase activity. After 2 weeks of incubation with polyesters, total DNA was extracted from the enrichment cultures and combined for the construction of the metagenomic fosmid libraries IS_Lib1 and IS_Lib2. In order to identify carboxylesterases with high-temperature profiles, this library was screened for esterase activity with tributyrin as the substrate (for carboxylesterases and lipases) at three temperatures: 37°C, 50°C, and 70°C. Emulsified tributyrin gave a turbid appearance to the plates, and the presence of active metagenomic esterases or lipases was seen as a clear zone around the colony. After screening 3,456 clones from the IS_Libr2 library on tributyrin agar plates, 64 positive hits were identified, with 19 positive clones observed at 37°C, 27 clones at 50°C, and 18 clones at 70°C. Furthermore, eight esterase-positive clones detected at 50°C were found to be unique for this temperature, whereas one unique clone was found at 70°C, suggesting that these esterases are mostly active only at elevated temperatures. Following endonuclease digestion profiling and Sanger sequencing analysis, 14 nonredundant fosmids were selected for insert sequencing using the Illumina platform, and fosmid inserts were assembled with an average size of 39 kbp. Sequence analysis revealed 12 putative open readings frames encoding predicted hydrolases (including peptidases, carboxylesterases, β-lactamases, serine proteases) homologous to proteins from *Chloroflexi* and metagenome-assembled genome affiliated with thermophilic *Chloroflexi*. From candidate proteins cloned in *E. coli*, three putative carboxylesterases (IS10, IS11, and IS12) were soluble when expressed in *E. coli* cells, and the presence of carboxylesterase activity in purified proteins was confirmed using a tributyrin agarose plates assay (Table 1), and proteins were further selected for detailed biochemical characterization. Amino acid sequences of IS10 (314 amino acids [aa]), IS11 (455 aa), and IS12 (318 aa) showed no presence of recognizable

TABLE 1 Novel carboxylesterases from the Ischia polyester enrichment metagenomes selected for biochemical and structural characterization in this study

Protein name	Fosmid ID	Protein length	Predicted MW	Protein superfamily	Host organism (phylum)
IS10	L2B6_15	314 aa	34.3 kDa	α/β-Hydrolase	*Chloroflexi*
IS11	L2F9_18	455 aa	49.4 kDa	β-Lactamase	*Chloroflexi*
IS12	L3G23_11	318 aa	33.9 kDa	α/β-Hydrolase	*Chloroflexi*

signal peptides. Both IS10 and IS12 belonged to the α/β-hydrolase superfamily and had 56.8% sequence identity to each other, whereas IS11 showed no significant sequence similarity to IS10 and IS12, as it is a member of the large family of β-lactamases and penicillin-binding proteins (Table 1). A BlastP search of the nrNCBI database revealed that amino acid sequences of IS10 and IS12 were identical to two putative α/β-hydrolases from uncultured *Chloroflexi* bacteria (GenBank accession numbers HEG24678.1 and HHR50377.1, respectively), whereas the IS11 sequence exhibited the highest identity (99.1%) to the putative class A β-lactamase-related serine hydrolase HDX58025.1 from uncultured *Dehalococcoidia*. Interestingly, the top homologous proteins of Ischia esterases were the proteins identified in the metagenome from a deep sea hydrothermal vent (black smoker) in the mid-Atlantic Ridge (South Atlantic Ocean) (38). The comparison with previously characterized proteins showed the thermostable arylesterase Are, from *Saccharolobus solfataricus* (UniProt ID B5BLW5, 306 aa) to be the top homologue for IS10 (42% sequence identity), whereas the metagenome-derived esterase Est8 (KP699699, PDB 4YPV; 348 aa) was the top characterized homologue for IS12 (56% sequence identity) (39, 40) (Fig. S2). The IS11 sequence was homologous to penicillin-binding proteins and β-lactamases with low sequence similarity to the CmcPBP from the *Actinobacteria Amycolatopsis lactamdurans* (Q06317; 36% identity) and esterase EstB from *Burkholderia gladioli* (Q9KX40; 32% identity) (41, 42). Domain and multiple sequence alignment confirmed the presence of conserved regions and motifs linked to esterase activity in lipolytic families previously described (Fig. S2 and S3). IS10 and IS12 contained an α/β-hydrolase fold (PF07859), displaying the characteristic catalytic triad composed of Ser155, Asp250, and His281 and the conserved consensus motif G-x-S-x-G around the active site serine (22), clustering together with representatives of family IV (Fig. S2 and S3).

The protein IS11 contained a β-lactamase domain (PF00144) and the consensus tetrapeptide S-x-x-K, which is perfectly conserved among all penicillin-binding enzymes and β-lactamases, surrounding the active serine Ser68. In addition, Lys71 and Tyr160 were also conserved as part of the catalytic triad of family VIII esterases, which groups enzymes with homology to class C β-lactamases and penicillin-binding proteins (Fig. S2 and S3).

Biochemical characterization of purified metagenomic carboxylesterases using model esterase substrates. The esterase activity of purified proteins (IS10, IS11, and IS12) was initially evaluated using model esterase substrates with different chain lengths (C_2 to C_{16}) at 30°C (to diminish spontaneous substrate degradation at high temperatures). The proteins were found to be active against several short acyl chain substrates, with IS10 and IS11 showing a preference to *p*-nitrophenyl (*p*NP)-butyrate, α-*N*-butyrate, and *p*NP-hexanoate, whereas IS12 was most active with *p*NP-acetate and α-*N*-propionate (Fig. 2). All enzymes were active within a broad pH range (pH 6.0 to 9.0), with maximal activities at pH 9 (Fig. S4a). The purified metagenomic carboxylesterases exhibited saturation kinetics with model esterase substrates at optimal pH 9.0 and 30°C (Table 2). IS10 appeared to be the most efficient esterase compared to IS11 and IS12, with the highest substrate affinity (lowest K_M) and catalytic efficiency (k_{cat}/K_M) toward the tested model substrates. IS12 showed higher substrate affinity to *p*NP-butyrate and higher activity with *p*NP-acetate than IS11, whereas the latter was more active against *p*NP-butyrate (Table 2).

Since the selected carboxylesterases originated from thermophilic environments, we investigated the effect of temperature on the activity (temperature profiles) and thermostability of purified carboxylesterases using *p*NP-butyrate as the substrate (Fig. 3).

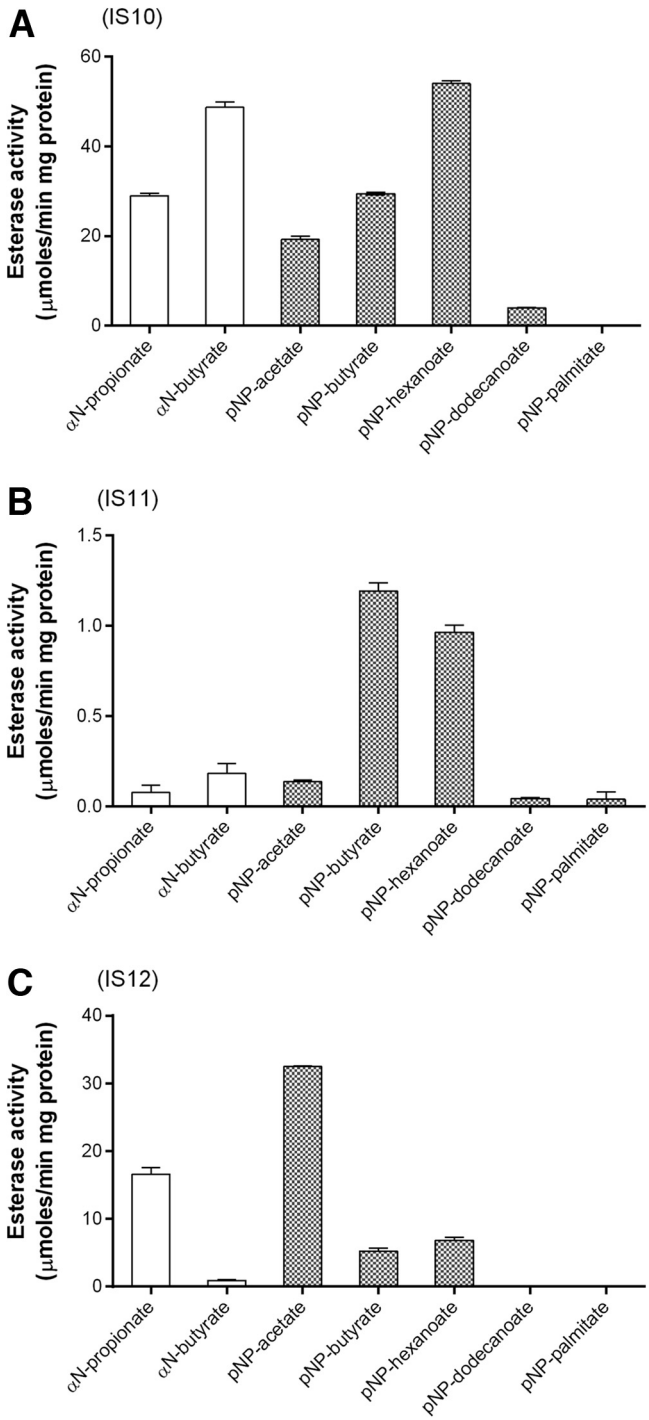

FIG 2 Hydrolytic activity of purified IS10 (A), IS11 (B), and IS12 (C) against model esterase substrates. The reaction mixtures contained the indicated *p*-nitrophenyl esters (*p*NP; white bars) and α-naphthyl esters (αN; gray bars) with different acyl chain lengths (reaction temperature 30°C) (see Materials and Methods for details).

All enzymes showed considerable activity at 20°C, but reaction rates increased 5 to 10 times at higher temperatures, with IS10 showing the highest activity at 60 to 70°C, whereas IS12 was most active at 70°C to 80°C and IS11 was most active at 80 to 90°C (Fig. 3). The thermostability of purified enzymes was analyzed using a 20-min preincubation at different temperatures (from 30 to 95°C) followed by esterase assays with *p*NP-butyrate at 30°C. IS10 retained 60% activity after preincubation at 50°C and showed a complete loss of activity at

TABLE 2 Kinetic parameters of purified metagenomic carboxylesterases from the Ischia hydrothermal vents with model esterase substrates[a]

Protein	Substrate	K_M (mM)	k_{cat} (s^{-1})	k_{cat}/K_M (s^{-1} M^{-1})
IS10	*p*NP-acetate	0.05 ± 0.01	41.97 ± 1.79	7.9×10^5
	*p*NP-butyrate	0.06 ± 0.01	66.21 ± 3.24	1.2×10^6
	*p*NP-hexanoate	0.04 ± 0.01	86.79 ± 3.06	2.0×10^6
	αN-propionate	0.06 ± 0.02	31.20 ± 1.93	5.0×10^5
	αN-butyrate	0.12 + 0.04	58.60 ± 5.89	4.9×10^5
IS11	*p*NP-acetate	0.53 ± 0.31	1.60 ± 0.30	3.0×10^3
	*p*NP-butyrate	0.20 ± 0.02	68.81 ± 1.37	3.5×10^5
	*p*NP-hexanoate	0.08 ± 0.02	40.28 ± 1.39	5.3×10^5
	αN-butyrate	0.09 ± 0.02	5.93 ± 0.49	6.9×10^4
IS12	*p*NP-acetate	0.22 ± 0.05	57.10 ± 3.78	2.6×10^5
	*p*NP-butyrate	0.08 ± 0.01	8.77 ± 0.29	1.1×10^5
	*p*NP-hexanoate	0.09 ± 0.01	19.05 ± 0.50	2.1×10^5
	αN-propionate	0.69 ± 0.19	39.45 ± 3.7	5.7×10^4

[a]Reaction conditions were as indicated in Materials and Methods (pH 9.0, 30°C). Results are means ± SD of three independent experiments. αN, α-naphthyl; *p*NP, *p*-nitrophenyl.

80°C (Fig. 3). In contrast, both IS11 and IS12 revealed a significant decrease of activity only after 20-min preincubation at 90°C and 70°C, respectively. After 2 h of incubation at 70°C, IS12 retained 50% of initial activity but was completely inactivated at 80°C (Fig. 4). However, IS11 showed no reduction or a small reduction of activity at 70°C and 80°C,

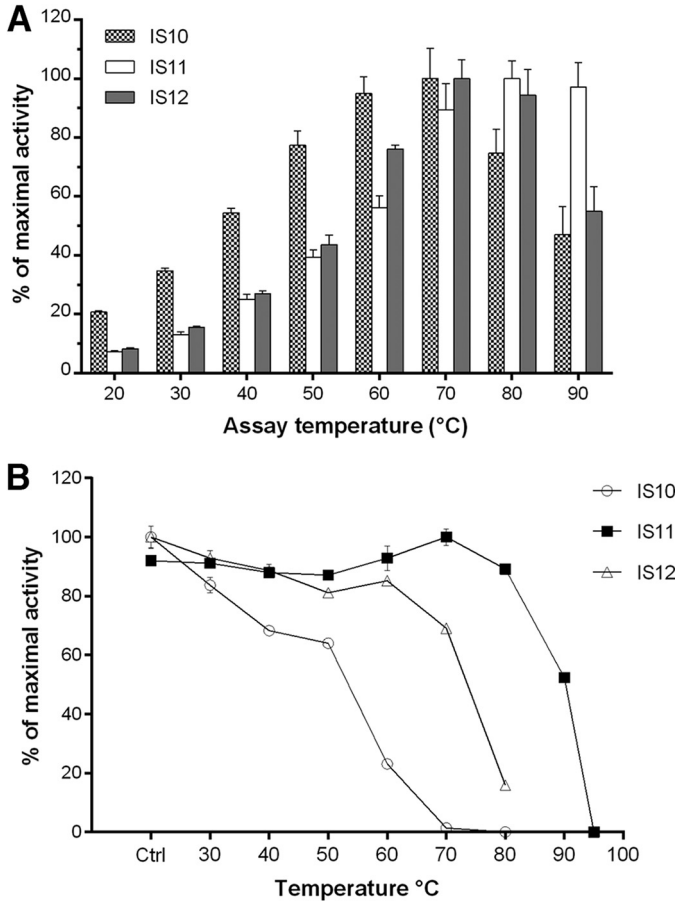

FIG 3 Activity temperature profiles and thermostability of purified metagenomic carboxylesterases from Ischia. (A) Esterase activity of purified enzymes with *p*NP-butyrate at different temperatures. (B) Thermostability of purified enzymes measured as residual activity after 20-min preincubation at different temperatures. Esterase activity was determined with *p*NP-butyrate as the substrate at 30°C. Ctrl, activity measured at 30°C without 20 min of preincubation.

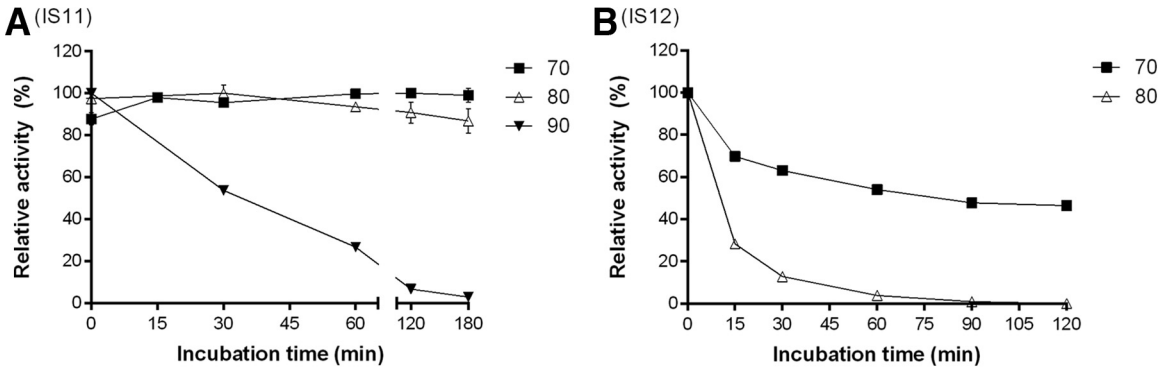

FIG 4 Thermoinactivation of purified IS11 (A) and IS12 (B) at different temperatures. Activity data are presented as relative activity from triplicate measurements ± standard deviations. Residual activity was determined with *p*NP-butyrate at 30°C.

respectively, and required over 3 h of incubation at 90°C for inactivation (Fig. 4). Thus, the metagenomic carboxylesterases from the Ischia hydrothermal vents are the thermophilic enzymes highly active at 70 to 80°C, with IS11 and IS12 also showing significant thermostability at temperatures from 60 to 80°C. Furthermore, the thermostability of IS11 and IS12 was comparable with, or exceeded, the thermostability of other esterases identified in high-temperature environments (43, 44–47).

Esterase activity of purified metagenomic esterases was inhibited by high concentrations of NaCl (50 to 67% of remaining activity in the presence of 0.5 M NaCl), with IS11 showing a slightly higher resistance (Fig. S4). Similarly, IS11 retained higher activity in the presence of nonionic detergents (43% and 53% in the presence of 2% Triton X-100 and Tween 20) (Fig. S4). With organic solvents, IS10 was inhibited by acetone, acetonitrile, ethanol, and isopropanol (10% [vol/vol]) (Fig. S5). In contrast, IS11 was more tolerant to these solvents (10 to 50%) and was stimulated by 10% ethanol (60% increase) and 30% methanol (84% increase). Furthermore, low concentrations of these solvents (10% [vol/vol]) stimulated esterase activity of IS12 (26 to 34% increase), whereas higher concentrations of acetone (50% [vol/vol]) and isopropanol (30% [vol/vol]) were inhibitory. Finally, dimethyl sulfoxide (10 to 30%) stimulated esterase activity of enzymes (20 to 46% increase) but was inhibitory to IS10 at 30% (Fig. S5).

Substrate range of purified carboxylesterases. To analyze the substrate range and preference of metagenomic carboxylesterases from the Ischia hydrothermal vents, the purified proteins were examined for the presence of hydrolytic activity against chemically and structurally diverse esters, including alkyl and aryl esters (see Materials and Methods). Both IS10 and IS12 revealed a broad substrate range with significant activity against all 44 tested ester substrates, and the highest activity with phenyl acetate, phenyl propionate, glyceryl tripropionate, tributyrin, and α-*N*-acetate (Table S2). IS12 was also highly active toward vinyl propionate. The broad substrate range of IS10 and IS12 correlated with relatively large effective volumes of their active sites, 650.23 Å^3 and 780.5 Å^3, respectively (calculated as cavity volume divided by solvent-accessible surface area) (23). These volumes are the largest calculated for prokaryotic esterases experimentally characterized so far, with only CalA lipase (Novozym 735) from the yeast *Candida antarctica* having a larger volume (23). IS11 had a more restricted substrate range, showing detectable activity against 22 ester substrates of 44 tested with a preference for benzyl (*R*)-(+)-2-hydroxy-3-phenylpropionate (Table S2). In this study, we found this ester was hydrolyzed by the three esterases (IS10, IS11, and IS12) but preferentially by IS11, suggesting that either the lipocalin domain of IS11 or the hydrophobic and polar residues located at the active site of this esterase (see structural features below) may have a role for the preference of this ester, not only in comparison with the other two esterases but also compared to other esters. The three metagenomic esterases revealed no apparent enantio-preference and hydrolyzed both enantiomers of several tested commercially available chiral substrates.

The purified metagenomic esterases were also tested for hydrolytic activity against the T-2 mycotoxin, which contains three ester groups on its side chains. The T-2 and

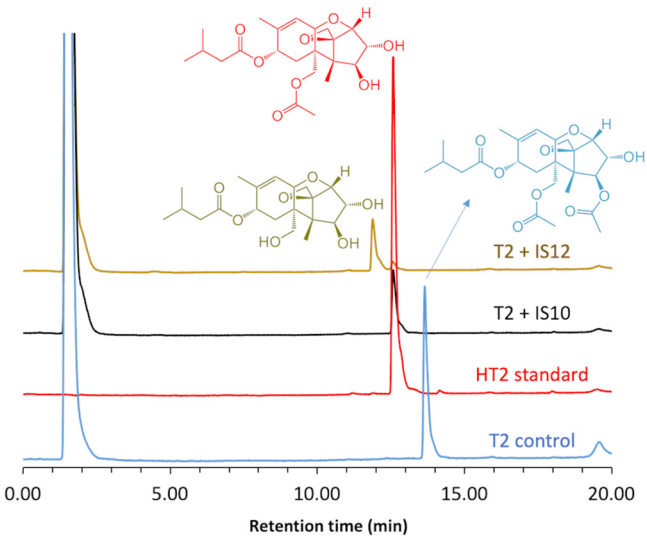

FIG 5 Hydrolytic activity of purified IS10 and IS12 against the mycotoxin T-2, determined by HPLC analysis of reaction products. Purified IS10 and IS12 were incubated with T-2 (at 37°C and pH 8.0), and reaction products were analyzed using HPLC (see Materials and Methods for experimental details).

deacetylated HT-2 toxins are members of the large group of trichothecene mycotoxins (over 190 derivatives) containing a tetracyclic ring system (48). Mycotoxins are highly toxic fungal metabolites that frequently contaminate food and feed and causing negative effects on human health, animals, and economy (49, 50). While physical and chemical methods have been used to detoxify mycotoxins, biological detoxification using enzymes or microbes is more attractive due to its specificity, safety, and costs. With T-2 as the substrate, both IS10 and IS12 showed high esterase activity based on a pH shift assay with phenol red (2.3 U/mg and 4.4 U/mg, respectively, at 37°C and pH 8.0), whereas IS11 was found to be inactive. Hydrolytic activity of IS10 and IS12 against T-2 was confirmed using high-performance liquid chromatography (HPLC), which also revealed the formation of different reaction products (Fig. 5). IS10 produced HT-2 as the main product, whereas HT-2 was present as the minor product in the reaction mixture with IS12, which produced mostly the T-2 triol as the main product (Fig. 5). Since the T-2 triol is known to be less toxic than T-2 and HT-2 (36, 51), IS12 might represent a promising candidate for the biodetoxification of T-2 and HT-2.

Since our metagenomic libraries were prepared using enrichment cultures with synthetic polyesters, the purified esterases were also tested for the presence of polyesterase activity. Although recent studies on biocatalytic depolymerization of synthetic polyesters, including PLA and polyethylene terephthalate (PET) have shown the potential of microbial carboxylesterases, there is an urgent need to identify novel robust polyesterases for applications in plastics recycling (35, 52, 53). The purified esterases were screened for the presence of polyesterase activity using an agarose plate assay with the emulsified PET model substrate bis(benzoyloxyethyl) terephthalate (3PET). These screens revealed the presence of polyesterase activity against 3PET in both IS10 and IS12, as indicated by the formation of a clear zone around the wells with loaded enzymes after incubation at 37°C (Fig. 6A). Purified IS11 did not show a visible clearance zone on the 3PET plate; however, the *in vitro* assay of hydrolysis of 3PET by IS11 and HPLC analysis of reaction products showed an increase in mono(2-hydroxyethyl) terephthalate (MHET), which was the main hydrolysis product, while IS10 and IS12 produced bis(2-hydroxyethyl) terephthalate (BHET) as the principal hydrolysis product (Fig. 6B). Furthermore, enzymes exhibited activity toward PLA, with a clear substrate preference toward poly-D,L-lactide [P(DL)A], over P(L)LA, over P(D)LA (Fig. 6C). To sum up, both IS10 and IS12 exhibited broad substrate profiles and were able to degrade both mycotoxins and polyesters.

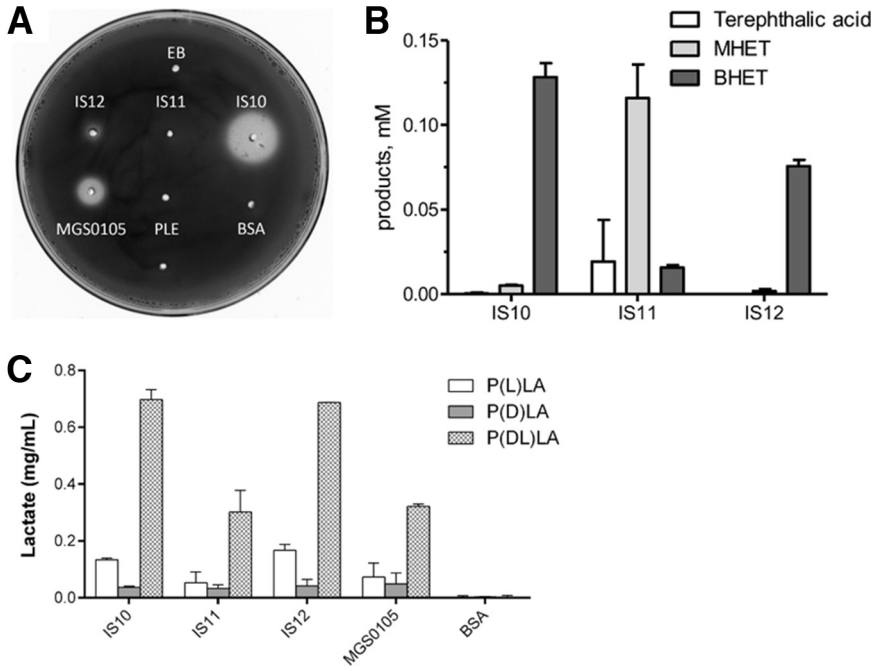

FIG 6 Polyesterase activity of metagenomic esterases against PLA and 3PET. (A) Plate assay with emulsified 3PET as the substrate. The formation of a clear zone around the wells with loaded enzyme indicates the presence of polyesterase activity. Agarose plates (1.5%) containing 0.2% emulsified 3PET and loaded proteins (50 μg/well) were incubated at 37°C and monitored for 3 days. Porcine liver esterase, bovine serum albumin, and elution buffer were used as negative controls, and esterase MGS0105, characterized previously (45), was a positive control. (B) HPLC assay of 3PET hydrolysis products after 16 h of incubation at 30°C; elution buffer was used as a negative control (not shown). (C) HPLC analysis of hydrolysis of PLA incubated with metagenomic esterases for 48 h at 30°C.

Structural studies of metagenomic carboxylesterases. To provide structural insights into the active site and activity of metagenomic carboxylesterases, purified proteins (IS10, IS11, and IS12) were subjected to crystallization trials. IS11 produced diffracting crystals, and its crystal structure was determined by molecular replacement (see Table S3 and Materials and Methods). The overall structure of IS11 revealed a protein dimer with protomers composed of two structural domains, an N-terminal β-lactamase-like serine hydrolase domain (aa 1 to 345) connected via a flexible linker (aa 346 to 358) to a C-terminal lipocalin domain (Fig. 7 and Fig. S6). Protein oligomerization has been suggested to contribute to thermostability of several thermophilic carboxylesterases (e.g., AFEst, PestE, EstE1) (33, 47, 54). Accordingly, the results of size exclusion chromatography of purified IS11, as well as that for IS10 and IS12, suggested that these proteins exist as dimers in solution (Fig. S7).

The serine β-lactamases (classes A, C, and D) are structurally and evolutionary related to penicillin-binding proteins (the targets of β-lactam antibiotics), which also include hydrolytic DD-peptidases (55, 56). The overall structure of the IS11 β-lactamase domain is composed of a mostly α-helical (all-α) subdomain inserted into an $\alpha/\beta/\alpha$ sandwich (or an α/β subdomain) (Fig. 7 and 8 and Fig. S6). The $\alpha/\beta/\alpha$ sandwich subdomain includes a nine-stranded antiparallel β-sheet flanked by two helices on each side, whereas the mostly helical subdomain comprises nine α-helices (Fig. 8). The search for structural homologues of IS11 using the Dali server (57) identified numerous β-lactamase-like proteins with low sequence identity, including the *Pyrococcus abyssi* peptidase PAB87 (PDB code 2QMI) and *Pseudomonas fluorescens* β-lactamase AmpC (PDB code 2QZ6) as the top structural homologues (Z scores of 36.0 to 40.2, root mean square deviation of 2.1 to 2.8 Å; sequence identity of 22 to 29%). The two subdomains form a groove accommodating the catalytic residues, including Ser68 (a nucleophile) and Lys71 (a general base accepting the proton from Ser68 O$^{\gamma}$) (first motif, S-x-x-K), Tyr160 and Asn162 (second motif, Y-x-N/S), and His299 (third motif, H/R/K-T/S/G-G). Accordingly, the IS11 structure revealed the presence of an additional electron density positioned near the side chains of Ser68, Tyr160, and His299, which represents

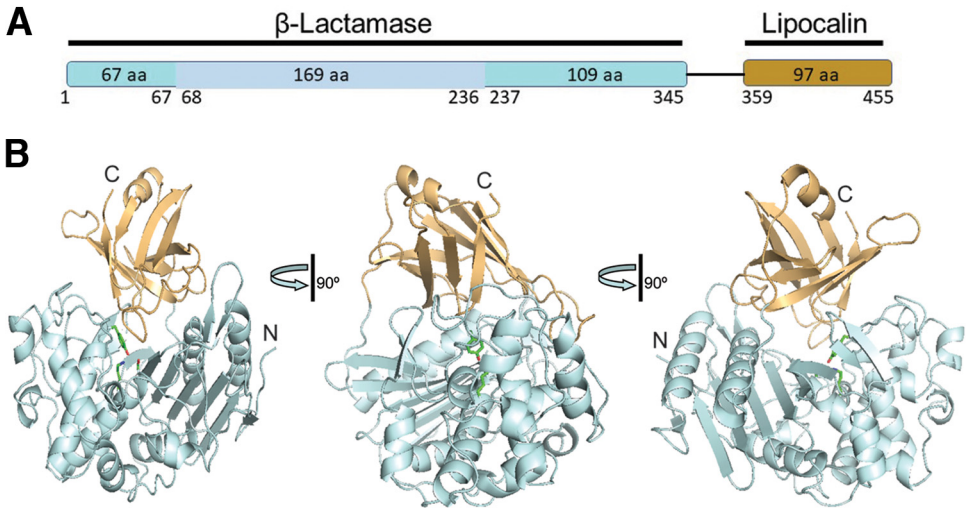

FIG 7 Crystal structure of IS11. (A) Schematic representation of the IS11 domains: the N-terminal β-lactamase-related Ser hydrolase domain is colored cyan with all-helical subdomain shown in light blue, whereas the C-terminal lipocalin domain is in orange. (B) Overall fold of the IS11 protomer shown in three views related by 90° rotations. The protein domains are shown as ribbon diagrams with the core domain (β-lactamase) colored pale cyan, whereas the C-terminal lipocalin domain is colored light orange. The position of the active site is indicated by the side chains of catalytic Ser68, Lys71, and Tyr160, whereas the protein N- and C-terminal ends are labeled (N and C).

an unknown ligand covalently attached to Ser68 (could not be modeled with various components of the protein purification or crystallization solutions) (Fig. 9A). The positioning of these catalytic residues was also conserved in the active sites of the biochemically characterized carboxylesterases with a β-lactamase fold (family VIII): EstB from *Burkholderia gladioli* and Pab87 from *Pyrococcus abyssi* (58, 59), suggesting a common catalytic mechanism with acylation-deacylation. The catalytic cleft of IS11 also contained several hydrophobic and polar residues potentially involved in substrate binding (Asp126, Phe128, Trp158, Asn304, Ile307, and Leu309) (Fig. 9).

The C-terminal domain of IS11 represents a typical lipocalin fold with one α-helix and an eight-stranded antiparallel β-barrel containing a hydrophobic core (Fig. 10). Lipocalins are a diverse family of small individual proteins or domains (160 to 180 aa) which bind various hydrophobic molecules (e.g., fatty acids) in a binding pocket located inside the barrel (60). Although lipocalins are very divergent in their sequences and functions, their structures exhibit remarkable similarity. The lipocalin α-helix of IS11 closes off the top of the β-barrel, whose interior represents a ligand-binding site coated mostly with hydrophobic residues (Fig. 10). In the IS11 protomer, the lipocalin domain covers the β-lactamase domain, shielding the catalytic cleft with an extended proline-rich strand (Pro391-Ser409) containing eight Pro residues (Pro391, Pro396, Pro401, Pro402, Pro404, Pro406, Pro407, and Pro408) (Fig. 10). In the thermophilic carboxylesterase Est2 from *Alicyclobacillus acidocaldarius*, the increased number of Pro residues has been suggested to be important for thermostability, because they reduce the flexibility of loops and other structural elements, making them more resistant to denaturation (61). The side chains of several residues of the lipocalin domain and proline-rich strand are positioned close to the IS11 active site, suggesting that they can be involved in substrate binding (Phe395, Arg397, Lys398, Arg403, and Arg449). Typical for all lipocalins, the interior of the IS11 β-barrel is coated by mostly hydrophobic and polar residues (Leu373, Ser374, Ile376, Leu387, Gln389, Leu426, Ser429, Phe444, Phe446, and Phe451). Proline-rich sequences are also known to be directly involved or facilitate protein-protein interactions or oligomerization (62). However, the IS11 dimer structure revealed no obvious interactions between the individual lipocalin domains (Fig. S6), suggesting that the lipocalin domain of IS11 participates in substrate binding rather than in the oligomerization.

High-quality structural models of IS10 and IS12 proteins constructed using the Phyre2 server (Fig. S8) revealed the presence of a core domain with a classical α/β-hydrolase fold

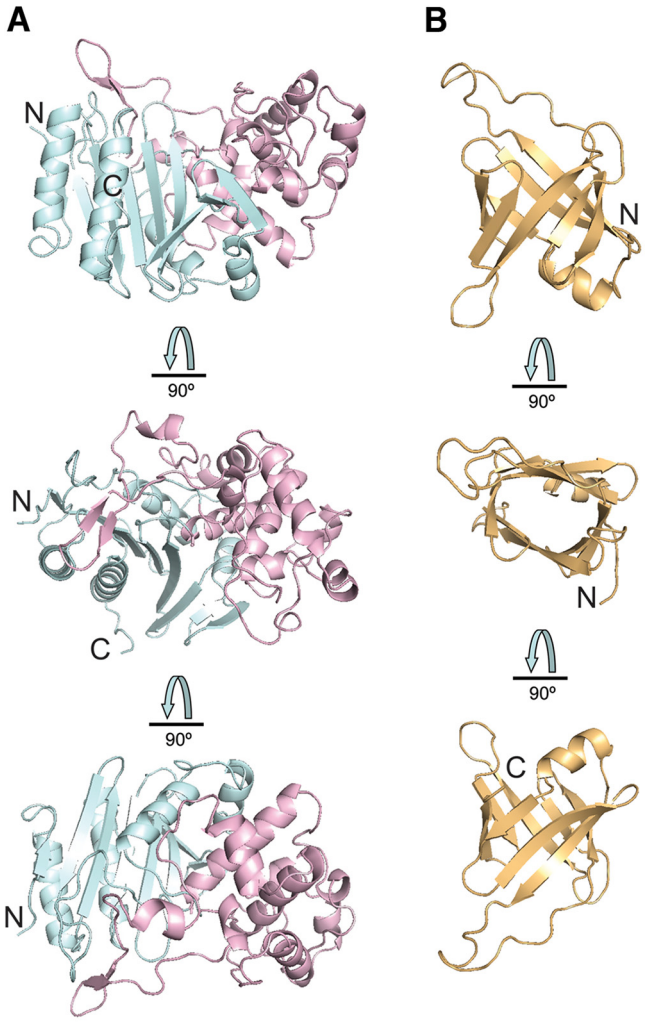

FIG 8 Crystal structure of the IS11 β-lactamase and lipocalin domains. (A) The N-terminal β-lactamase-like domain with two subdomains are colored pale cyan (α/β) and light pink (all-helical). (B) The lipocalin domain. The domains are shown in three views related by 90° rotations with the N and C termini labeled (N and C).

and an all-helical domain, as well as a serine hydrolase catalytic triad (Ser155, His280, and Asp250) in both proteins (Fig. S9). The putative catalytic nucleophile Ser155 is located on the classical nucleophilic elbow, a short sharp turn between a β-strand and α-helix. It is located at the bottom of the active site, which is mostly covered by the all-helical lid domain (Fig. S9). Both acyl- and alcohol-binding pockets of IS10 and IS12 include several hydrophobic and polar residues potentially involved in substrate binding (IS10: His81, Trp85, His93, Asn159, Tyr183, Val185, Leu252; IS12: Trp85, Ile87, His93, Asn159, Tyr183, Leu252, Ile279, Val283, Thr284, Leu285) (Fig. S9). Furthermore, the lid domains of both enzymes contain additional hydrophobic residues, which can contribute to substrate binding (IS10: Phe34, Met38, Phe203, Leu204, Met208, Met209, and Tyr211; IS12: Phe22, Met34, Tyr195, Leu203, Leu204, Met209, Phe212, and Trp213).

Conclusions. The present work demonstrated the high value of high-temperature microbial habitats, particularly those on the volcanic island of Ischia (Italy), the Terme di Cavascura and Maronti Beach hydrotherms, populated by taxonomically diverse microorganisms, as a resource for discovery of high-temperature active enzymes. As revealed by an in-depth characterization of three metagenomics-derived carboxylesterases (IS10, IS11, and IS12), they were active at temperatures as high as 70 to 90°C and were capable of degrading bio-based and synthetic polyester plastics. 3PET was

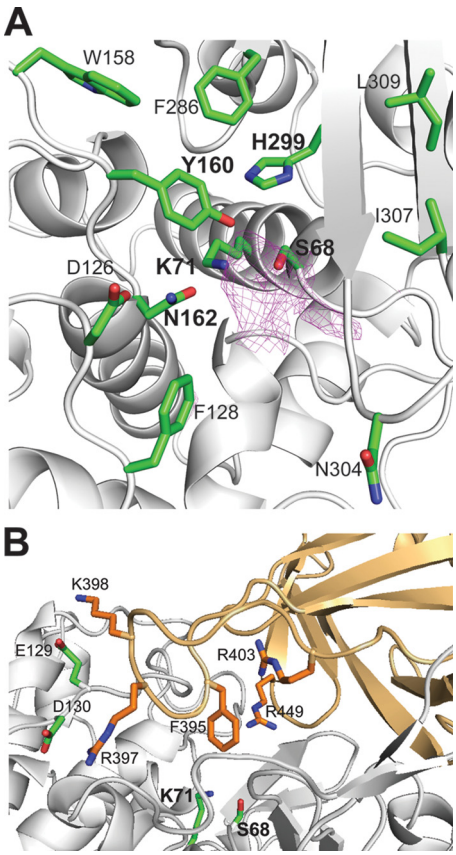

FIG 9 Close-up view of the IS11 active site. (A) The core domain showing the active site cleft with catalytic residues: motif-1 (Ser68 and Lys71), motif-2 (Tyr160 and Asn162), and motif-3 (His299). The magenta-colored mesh represents an additional electron density (a 2Fo-Fc omit map contoured at 2.5 σ) covalently attached to the Ser68 side chain. (B) The proline-rich loop of the lipocalin domain covering the active site and residues potentially contributing to substrate binding. Protein ribbon diagrams are colored gray (the β-lactamase domain) and light orange (the lipocalin domain), whereas the side chains of residues are shown as sticks with green and orange carbons, respectively.

hydrolyzed by IS10 and IS12 to predominantly BHET, while IS11 produced MHET as a main product. Interestingly, IS12 further degraded mycotoxin T-2, a common agent causing poisoning of animal feeds, to the less toxic T-2 triol. The three wild-type enzymes may be readily applicable in pilot trials in industrial processes relevant to the

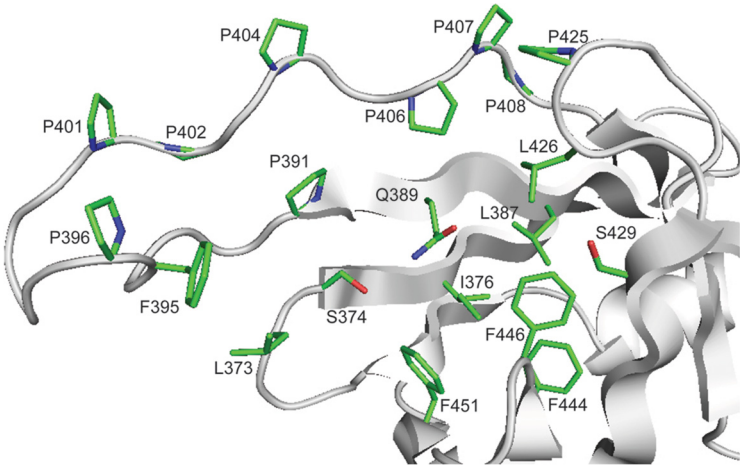

FIG 10 Crystal structure of the IS11 lipocalin domain ligand binding site and proline-rich loop. The protein ribbon diagram is colored in gray with the residues of the ligand-binding pocket shown as sticks with green carbons and labeled.

circular bioeconomy for plastics and/or in the production of toxin-free foods and feeds. This study could also serve as a starting point for deepening our knowledge on structural determinants for substrate specificity in carboxylesterases and for rational engineering to further improve their catalytic efficiencies to make accepting PET oligomers larger than 3PET.

MATERIALS AND METHODS

Environmental sampling sites and enrichment cultures. Sediment samples with water were collected in September 2018 from the geothermal areas of the volcanic island of Ischia (Gulf of Naples, Italy). The samples were taken from the Cavascura hydrothermal springs (latitude 40.70403, longitude 13.90502), IS1 (pH 8.5, 45°C) and IS2 (pH 7.0, 55°C), and from the sandy fumaroles of Maronti Beach near St. Angelo (latitude 40.70101, longitude 13.89837), IS3 (pH 4.5, 75°C) and IS4 (pH 5.0, 75°C). For each sample, triplicate enrichment cultures were established containing different polymers or plastics as the substrates, polylactic acid film (PLA [poly-D,L-lactide], M_w 10,000 to 18,000 Da), PHB, and a commercial compostable polyester blend (P3 blend), kindly provided by the Biocomposites Centre, Bangor University, United Kingdom. Plastic films that had been cut (3 mm by 20 mm), washed in 70% ethanol, and air dried were added to samples. For IS1 and IS2 cultures, modified DSMZ medium 1374 (https://bacmedia.dsmz.de/medium/1374) was used, which contained (g liter^{-1}): NaCl, 1; $MgCl_2 \cdot 6H_2O$, 0.4; KCl, 0.1; NH_4Cl, 0.25; KH_2PO_4, 0.2; Na_2SO_4, 4; $NaHCO_3$, 0.1; $CaCl_2 \cdot 2H_2O$, 0.5. The medium was adjusted to pH 7.5 with 10 N NaOH. For IS3 and IS4 cultures, modified DSMZ medium 88 (https://bacmedia.dsmz.de/medium/88) was used, which contained (g liter^{-1}): $(NH_4)_2SO_4$, 1.3; KH_2PO_4, 0.28; $MgSO_4 \cdot 7H_2O$, 0.25; $CaCl_2 \cdot 2H_2O$, 0.07. The medium was adjusted to pH 4.5 with 10 N H_2SO_4. Additionally, the trace element solution SL-10 (from DSMZ medium 320 https://bacmedia.dsmz.de/medium/320) was added at 1:1,000 (vol/vol) to both media. Enrichment cultures contained 0.5 g of sample sediment and 0.25 g of a polymer in 10 mL of growth medium. The cultures were incubated at 50°C (IS1 and IS2) or 75°C (IS3 and IS4) with slow agitation (30 rpm) for 4 days, and then culture aliquots (20% of the volume of enrichment cultures) were transferred to a fresh medium and incubated for 11 days under the same conditions (Table S1).

DNA extraction and 16S rRNA amplicon sequencing. Prior to DNA extraction, the enrichment cultures (9 mL each) were vortexed and biomass was collected by centrifugation at 10,000 relative centrifugal force for 10 min at 4°C. The pellets were resuspended in 250 μL of sterile phosphate-buffered saline (pH 7.5) and transferred to 1.5-mL tubes. High-molecular-weight DNA was obtained using the ZymoBIOMICS DNA Miniprep kit (Zymo Research, Irvine, CA, USA) in accordance with the manufacturer's instructions. Finally, DNA was eluted with 50 μL of nuclease-free water. The quality of extracted DNA was assessed by gel electrophoresis, and DNA concentration was estimated using a Qubit 4.0 fluorometer dsDNA BR assay kit (Life Technologies, USA). The Illumina-compatible libraries of hypervariable V4 region of 16S rRNA gene were prepared by single PCR with dual-indexing primer system with heterogeneity spacer as described previously (63). Modified forward primer F515 (5′-GTGBCAGCMGCCGCGGTAA-3′) and reverse R806 prokaryotic primer (5′-GGACTACHVGGGTWTCTAAT-3′) were used. PCRs were performed using MyTaq Red DNA polymerase (Bioline) in a Bio-Rad thermocycler with the following program: 95°C for 2 min for denaturation, followed by 30 cycles at 95°C for 45 s, 50°C for 60 s, and 72°C for 30 s, with a final elongation at 72°C for 3 min. PCR products of approximately 440 bp were visualized by gel electrophoresis and gel-purified using the QIAEX II gel extraction kit (Qiagen). The purified barcoded amplicons were quantified by using the Qubit dsDNA BR assay kit (Life Technologies, USA), pooled in equimolar amounts, and sequenced on the Illumina MiSeq platform (Illumina Inc., San Diego, CA, USA) using paired-end 250-bp reads at the Centre for Environmental Biotechnology (Bangor, United Kingdom). Sequencing reads were processed and analyzed as previously described (64). All statistical analysis was conducted using the R programming environment (65) *prcomp* function and in-house scripts for graphical design.

Preparation of the Ischia metagenome library from polyester enrichment cultures. High-molecular-weight DNA extracted from all enrichment cultures was combined in equimolar amounts and used to prepare two metagenomic fosmid libraries, IS_Lib1 (Cavascura enrichments) and IS_Lib2 (Maronti enrichments) using the CopyControl fosmid library pCC2FOS production kit (Epicentre Technologies, Madison, WI, USA). DNA was end-repaired to generate blunt-ended 5′-phosphorylated fragments according to the manufacturer's instructions. Subsequently, DNA fragments in the range of 30 to 40 kbp were resolved by gel electrophoresis (2 V cm^{-1} overnight at 4°C) and recovered from 1% low-melting-point agarose gel using GELase 50× buffer and GELase enzyme (Epicentre). Nucleic acid fragments were then ligated to the linearized CopyControl pCC2FOS vector following the manufacturer's instructions. After the *in vitro* packaging into the phage lambda (MaxPlax lambda packaging extract, Epicentre), the transfected phage T1-resistant EPI300-T1^R *E. coli* cells were spread on Luria-Bertani (LB) agar medium containing 12.5 μg mL^{-1} chloramphenicol and incubated at 37°C overnight to determine the titer of the phage particles. The resulting libraries had estimated titers of 14×10^4 and 1×10^4 nonredundant fosmid clones in the IS_Lib1 and IS_Lib2 libraries, respectively. For long-term storage, *E. coli* colonies were washed from the agar surface using liquid LB medium containing 20% (vol/vol) sterile glycerol, and the aliquots were stored at −80°C.

Activity-based screening of the polyester enrichment metagenome library for esterase activity. The metagenomic libraries were screened for carboxylesterase and lipase activity as follows. The fosmid library was grown on LB agar plates containing 12.5 μg mL^{-1} chloramphenicol at 37°C overnight to yield single colonies. Then, 3,456 clones were arrayed in 9- by 384-well microtiter plates and cultivated at 37°C in LB medium supplemented with 12.5 μg mL^{-1} chloramphenicol. Those original microtiter plates

were stored at −80°C after the addition of glycerol, at a final concentration of 20% (vol/vol). For screening clone libraries, 384-pin replicators were used to print clones onto the surface of large LB agar square plates (245 mm by 245 mm) containing 12.5 μg mL^{-1} chloramphenicol, and 2 mL liter^{-1} fosmid autoinduction solution (Epicentre), and each plate contained 0.3% (vol/vol) tributyrin (Sigma-Aldrich, Gillingham, United Kingdom) as described previously (27). After an initial overnight growth at 37°C, the LB agar plates were incubated for 48 h at 37, 50, or 70°C. Positive hits were confirmed by retesting the corresponding fosmid clones taken from the original microtiter plate.

Sequencing and analysis of metagenomic fragments. Positive fosmid clones were cultivated in 100 mL LB medium containing 12.5 μg mL^{-1} chloramphenicol and 2 mL liter^{-1} fosmid autoinduction solution (Epicentre) at 37°C overnight. Biomass was collected by centrifuging at 3,200 $\times$ *g* for 30 min, and fosmid DNA was extracted from the pellet using the Qiagen Plasmid Midi kit (Qiagen) following the manufacturer's instructions. Approximate sizes of the cloned fragments were assessed on agarose gel electrophoresis after double endonuclease digestion with XbaI and XhoI (New England Biolabs, Ipswich, MA, USA). The Sanger sequencing of the termini of inserted metagenomic fragments of each purified fosmid was done at Macrogen Ltd. (Amsterdam, The Netherlands) using standard pCC2FOS sequencing primers (Epicentre). Nonredundant fosmids were selected, their DNA concentrations were quantified by a Qubit 4.0 Fluorometer dsDNA BR assay kit (Invitrogen), pooled in equimolar amounts, and prepared for Illumina MiSeq sequencing. Pooled DNA was fragmented using the Bioruptor Pico sonicator (Diagenode, Denville, NJ, USA) with parameters adjusted to obtain 400- to 600-bp fragments. The fragment library was prepared using the NEBNext Ultra II DNA library preparation kit (New England Biolabs, Ipswich, MA, USA) according to the manufacturer's instructions. The obtained library was sequenced on the MiSeq platform (Illumina, San Diego, USA) using a microflow cell 300-cycle V2 sequencing kit. Obtained paired-end reads were subjected to quality filtering, trimming, and assembly as previously described (43). Gene prediction and primary functional annotation were performed using the MetaGeneMark annotation software (http://opal.biology.gatech.edu) (66). Translated protein sequences were annotated using BLAST searches of UniProt and the nonredundant GenBank databases (67). Multiple sequence alignments were generated using the MUSCLE application (68) and visualized with Geneious v.9 (Biomatters, New Zealand). The neighbor-joining and maximum likelihood trees were constructed in MEGA X (69) using the settings for the Poisson model and homogenous patterning between lineages. The bootstrapping was performed with 1,000 pseudoreplicates.

Gene cloning, expression, and purification of selected proteins. Selected gene candidates were amplified by PCR in a T100 thermal cycler (Bio-Rad) using Herculase II fusion enzyme (Agilent, Cheadle, United Kingdom) with oligonucleotide primer pairs incorporating pET-46 Ek/LIC vector adapters (Merck, Darmstadt, Germany). PCR products were then purified and cloned into the above pET-46 Ek/LIC vector harboring an N-terminal 6$\times$ His tag, as described by the manufacturer. The DNA inserts in the resulting plasmids were verified by Sanger sequencing at Macrogen Ltd. (Amsterdam, The Netherlands) and then transformed into *E. coli* BL21(DE3) for recombinant protein expression. *E. coli* BL21(DE3) harboring pET-46 Ek/LIC plasmid was grown on LB medium to mid-log growth phase (optical density at 600 nm, 0.7 to 0.8), induced with isopropyl-β-D-thiogalactopyranoside (0.5 mM), and incubated at 20°C overnight. Cells were disrupted by sonication as reported earlier (70), and recombinant proteins were purified using metal-chelate affinity chromatography on Ni-nitrilotriacetic acid His-bind columns. Protein size and purity were assessed using denaturing gel electrophoresis (SDS-PAGE), and protein concentration was measured by Bradford assay (Merck, Gillingham, United Kingdom).

Enzyme assays. Carboxyl esterase activity of purified proteins against *p*-nitrophenyl (*p*NP) or α-naphthyl (αN) esters was determined by measuring the amount of α-naphthol released by esterase-catalyzed hydrolysis, essentially as described previously (27, 70). Under standard assay conditions, the reaction mixture contained 50 mM potassium phosphate buffer (pH 7.0), 1 mM *p*NP-butyrate as the substrate, and 0.2 to 1.8 μg of enzyme in a final volume of 200 μL. Reaction mixtures were incubated at 30°C for 3 to 5 min and monitored at 410 nm (for *p*NP esters) or 310 nm (for αN esters). Nonenzymatic hydrolysis of ester substrates was subtracted using a blank reaction with denatured enzyme. The effect of pH on esterase activity was evaluated using the following buffers: sodium citrate (pH 4.0 and 5.0), potassium phosphate (pH 6.0 and 7.0), and Tris-HCl (pH 8.0 and 9.0). The activity was monitored at 348 nm (the pH-independent isosbestic wavelength of α-naphthol). The effect of temperature on esterase activity was studied using a range of temperatures (from 20°C to 90°C). In order to assess the thermal stability of purified esterases, the enzymes were dissolved in potassium phosphate buffer (pH 7.0) and preincubated at the indicated temperatures (from 30 to 95°C) for 20 min. The enzyme solutions were then cooled on ice, and the residual activity was measured under standard conditions (at 30°C). Substrate specificity of purified enzymes was analyzed using model *p*NP- and αN-esters with different chain lengths: *p*NP-acetate (C_2), αN-propionate (C_3), *p*NP-butyrate (C_4), αN-butyrate (C_4), *p*NP-hexanoate (C_6), *p*NP-dodecanoate (C_{12}), and *p*NP-palmitate (C_{16}), obtained from Sigma-Aldrich and Tokyo Chemical Industry TCI. Kinetic parameters for these substrates were determined over a range of substrate concentrations (0.012 to 4 mM; 30°C) and calculated by nonlinear regression analysis of raw data fit to the Michaelis-Menten function using GraphPad Prism software v.6. Hydrolysis of 44 soluble nonchromogenic monoester substrates (Table S2) and T-2 mycotoxin (Merck Life Science S.L.U., Madrid, Spain) was assayed at 37°C using a pH indicator assay with phenol red and monitored at 550 nm (71). The reaction products of enzymatic degradation of T-2 mycotoxin were analyzed using reversed-phase chromatography on a Waters 600 HPLC system, coupled to an autosampler (Waters model 717plus), equipped with a Zorbax Eclipse Plus C_{18} column (Agilent, 4.6 by 100 mm, 3.5 μm, 40°C) and an evaporative light-scattering detector (Sedere Sedex model 55). The reaction products were separated using gradient elution (1.0 mL/min) with acetonitrile and water (5% for 1 min, 5% to 95% for 9 min, 95% for 3 min, and 5% for 7 min). Polyester depolymerization activity of purified proteins against 3PET was measured using 1.5% agarose plates containing 0.2% of emulsified polyesters. 3PET was purchased from CanSyn Chem. Corp. (Toronto, Canada). Agarose plates with

emulsified 3PET were prepared as described previously (52). After protein loading, the plates were sealed and incubated at 37°C for 1 to 5 days. The presence of polyesterase activity was indicated by the formation of a clear zone around the wells with proteins. Apart from plate assays, activity assays of IS10, IS11, and IS12 for 3PET suspension hydrolysis were performed in 50 mM Tris-HCl buffer (pH 8.0) at 30°C in a shaker at 600 rpm, the final reaction volume for each experiment was 0.2 mL, and the final protein amount was 50 μg. The reactions were terminated after 13 h by filtering reaction mixture on a 10-kDa spin filter. Ten microliters of filtrate was analyzed using the HPLC Schimadzu Prominence-I system (Milton Keynes, United Kingdom) equipped with a Schimadzu C_{18} Shim-pack column (4.6 by 150 mm, 5 μm). The mobile phase was 25% (vol/vol) methanol with 0.1% (vol/vol) H_3PO_4 in HPLC-grade water at a flow rate of 0.7 mL min^{-1} for 2 min, followed by an increase to 55% methanol to 118 min, then 25% methanol at 22 min; the effluent was monitored at a wavelength of 240 nm, and the column was conditioned at 40°C. The hydrolytic products of MHET, BHET, and TPA were identified by comparing the retention times with their standards, and reactions without enzyme served as negative controls. All samples of each experiment were analyzed in triplicate.

Enzymatic activity against PLA. Hydrolysis of PLA was assayed by measurement of lactic acid production as follows. Five milligrams each of PLA (all were acid-terminated and purchased from PolySciTech [West Lafayette, IN, USA]; P(D)LA at 10 to 15,000 Da, P(D,L)LA [Resomer R202H; at 10 to 18,000 Da], or P(L)LA at 15 to 25,000 Da) suspended in 0.5 mL of 0.4 M Tris-HCl (pH 8.0) were mixed with 50 μg of purified enzyme and incubated for 48 h at 37°C with shaking (1,000 rpm). Samples were then centrifuged at 12,000 $\times$ *g* for 5 min at 4°C. A 200-μL aliquot of supernatant was mixed with 200 μL of mobile phase (0.005 N H_2SO_4). Sample was filtered through 13-mm Millipore PES syringe membrane filters (0.02-μm pore diameter) and analyzed on an HPLC Shimadzu, Prominence-I (Milton Keynes, United Kingdom) with an ion exchange column, Hi PlexH (300 by 7.7 mm; Agilent, Cheadle, United Kingdom) and 0.6 mL min^{-1} flow rate at 55°C (oven temperature) with UV detector set at 190 to 210 nm.

Protein crystallization and structure determination. Native metagenomic esterases were purified using metal-chelate affinity chromatography, and crystallization was performed at room temperature using the sitting-drop vapor diffusion method. For IS11, protein concentration was 25 mg mL^{-1}, reservoir solution was 0.1 M citric acid, pH 3.5, and 19% polyethylene glycol 3350. The crystal was cryoprotected by transferring into paratone oil and then flash-frozen in liquid nitrogen. Diffraction data for the IS11 crystal were collected at 100 K with a Rigaku Home Source Micromax-007 with an R-AXIS IV++ detector and processed using HKL3000 (72). The structure was solved by molecular replacement using Phenix.phaser (73) and a model built with AlphaFold2 (74). Model building and refinement were performed using Phenix.refine and Coot (75). Translation/libration/screw parameterization was utilized for refinement, and *B*-factors were refined as isotropic. Structure geometry and validation were performed using the Phenix Molprobity tools. Data collection and refinement statistics for this structure are summarized in Table S3.

Data availability. Small subunit rRNA gene sequences were deposited to GenBank as BioProject ID PRJNA881593. Sequences of IS10, IS11, and IS12 proteins were deposited to GenBank under accession numbers OL304252, OL304253, and OL304254. The atomic coordinates of IS11 have been deposited in the Protein Data Bank with accession code 7SPN.

SUPPLEMENTAL MATERIAL

Supplemental material is available online only.

SUPPLEMENTAL FILE 1, PDF file, 2.8 MB.

ACKNOWLEDGMENTS

This study was conducted under the auspices of the FuturEnzyme Project funded by the European Union's Horizon 2020 Research and Innovation Program under grant agreement 101000327. M.F. and F.J.P. also acknowledge grants PID2020-112758RB-I00 (M.F.), PDC2021-121534-I00 (M.F.), TED2021-130544B-I00 (M.F.), and PID2019-105838RB-C31 (F.J.P.) from MCIN/AEI/10.13039/501100011033 and the European Union ("NextGenerationEU/PRTR"). M.A.D., T.N.C., R.B., A.N.K., O.V.G., A.F.Y., and P.N.G. are thankful for support from the European Regional Development Fund (ERDF) through the Welsh Government to the Centre for Environmental Biotechnology, project number 81280. P.N.G. and A.F.Y. acknowledge the Natural Environment Research Council UK-funded Plastic Vectors project NE/S004548/1 and the Sêr Cymru program partly funded by the ERDF through the Welsh Government for support of the project BioPOL4Life. We are indebted to Connie Tulloch and Gwion Williams for their technical support.

REFERENCES

1. Kyrpides NC, Hugenholtz P, Eisen JA, Woyke T, Göker M, Parker CT, Amann R, Beck BJ, Chain PSG, Chun J, Colwell RR, Danchin A, Dawyndt P, Dedeurwaerdere T, DeLong EF, Detter JC, De Vos P, Donohue TJ, Dong X-Z, Ehrlich DS, Fraser C, Gibbs R, Gilbert J, Gilna P, Glöckner FO, Jansson JK, Keasling JD, Knight R, Labeda D, Lapidus A, Lee J-S, Li W-J, Ma J, Markowitz V, Moore ERB, Morrison M, Meyer F, Nelson KE, Ohkuma M, Ouzounis CA, Pace N, Parkhill J, Qin N, Rossello-Mora R, Sikorski J, Smith D, Sogin M, Stevens R, Stingl U, Suzuki K-I, et al. 2014. Genomic encyclopedia of bacteria and archaea: sequencing a myriad of type strains. PLoS Biol 12:e1001920. https://doi.org/10.1371/journal.pbio.1001920.
2. Yarza P, Yilmaz P, Pruesse E, Glockner FO, Ludwig W, Schleifer KH, Whitman WB, Euzeby J, Amann R, Rossello-Mora R. 2014. Uniting the classification of cultured and uncultured bacteria and archaea using 16S rRNA gene sequences. Nat Rev Microbiol 12:635–645. https://doi.org/10.1038/nrmicro3330.

3. Rappe MS, Giovannoni SJ. 2003. The uncultured microbial majority. Annu Rev Microbiol 57:369–394. https://doi.org/10.1146/annurev.micro.57.030502.090759.
4. Torsvik V, Goksoyr J, Daae FL. 1990. High diversity in DNA of soil bacteria. Appl Environ Microbiol 56:782–787. https://doi.org/10.1128/aem.56.3.782-787.1990.
5. Handelsman J. 2004. Metagenomics: application of genomics to uncultured microorganisms. Microbiol Mol Biol Rev 68:669–685. https://doi.org/10.1128/MMBR.68.4.669-685.2004.
6. Ferrer M, Golyshina O, Beloqui A, Golyshin PN. 2007. Mining enzymes from extreme environments. Curr Opin Microbiol 10:207–214. https://doi.org/10.1016/j.mib.2007.05.004.
7. Uchiyama T, Miyazaki K. 2009. Functional metagenomics for enzyme discovery: challenges to efficient screening. Curr Opin Biotechnol 20:616–622. https://doi.org/10.1016/j.copbio.2009.09.010.
8. Turnbaugh PJ, Gordon JI. 2008. An invitation to the marriage of metagenomics and metabolomics. Cell 134:708–713. https://doi.org/10.1016/j.cell.2008.08.025.
9. Venter JC, Remington K, Heidelberg JF, Halpern AL, Rusch D, Eisen JA, Wu D, Paulsen I, Nelson KE, Nelson W, Fouts DE, Levy S, Knap AH, Lomas MW, Nealson K, White O, Peterson J, Hoffman J, Parsons R, Baden-Tillson H, Pfannkoch C, Rogers YH, Smith HO. 2004. Environmental genome shotgun sequencing of the Sargasso Sea. Science 304:66–74. https://doi.org/10.1126/science.1093857.
10. Rusch DB, Halpern AL, Sutton G, Heidelberg KB, Williamson S, Yooseph S, Wu D, Eisen JA, Hoffman JM, Remington K, Beeson K, Tran B, Smith H, Baden-Tillson H, Stewart C, Thorpe J, Freeman J, Andrews-Pfannkoch C, Venter JE, Li K, Kravitz S, Heidelberg JF, Utterback T, Rogers YH, Falcón LI, Souza V, Bonilla-Rosso G, Eguiarte LE, Karl DM, Sathyendranath S, Platt T, Bermingham E, Gallardo V, Tamayo-Castillo G, Ferrari MR, Strausberg RL, Nealson K, Friedman R, Frazier M, Venter JC. 2007. The Sorcerer II Global Ocean Sampling expedition: northwest Atlantic through eastern tropical Pacific. PLoS Biol 5:e77. https://doi.org/10.1371/journal.pbio.0050077.
11. Yooseph S, Sutton G, Rusch DB, Halpern AL, Williamson SJ, Remington K, Eisen JA, Heidelberg KB, Manning G, Li W, Jaroszewski L, Cieplak P, Miller CS, Li H, Mashiyama ST, Joachimiak MP, van Belle C, Chandonia JM, Soergel DA, Zhai Y, Natarajan K, Lee S, Raphael BJ, Bafna V, Friedman R, Brenner SE, Godzik A, Eisenberg D, Dixon JE, Taylor SS, Strausberg RL, Frazier M, Venter JC. 2007. The Sorcerer II Global Ocean Sampling expedition: expanding the universe of protein families. PLoS Biol 5:e16. https://doi.org/10.1371/journal.pbio.0050016.
12. Qin J, Li R, Raes J, Arumugam M, Burgdorf KS, Manichanh C, Nielsen T, Pons N, Levenez F, Yamada T, Mende DR, Li J, Xu J, Li S, Li D, Cao J, Wang B, Liang H, Zheng H, Xie Y, Tap J, Lepage P, Bertalan M, Batto JM, Hansen T, Le Paslier D, Linneberg A, Nielsen HB, Pelletier E, Renault P, Sicheritz-Ponten T, Turner K, Zhu H, Yu C, Li S, Jian M, Zhou Y, Li Y, Zhang X, Li S, Qin N, Yang H, Wang J, Brunak S, Doré J, Guarner F, Kristiansen K, Pedersen O, Parkhill J, Weissenbach J, MetaHIT Consortium, et al. 2010. A human gut microbial gene catalogue established by metagenomic sequencing. Nature 464:59–65. https://doi.org/10.1038/nature08821.
13. Hess M, Sczyrba A, Egan R, Kim TW, Chokhawala H, Schroth G, Luo S, Clark DS, Chen F, Zhang T, Mackie RI, Pennacchio LA, Tringe SG, Visel A, Woyke T, Wang Z, Rubin EM. 2011. Metagenomic discovery of biomass-degrading genes and genomes from cow rumen. Science 331:463–467. https://doi.org/10.1126/science.1200387.
14. Ferrer M, Martínez-Martínez M, Bargiela R, Streit WR, Golyshina OV, Golyshin PN. 2016. Estimating the success of enzyme bioprospecting through metagenomics: current status and future trends. Microb Biotechnol 9:22–34. https://doi.org/10.1111/1751-7915.12309.
15. Levitt M. 2009. Nature of the protein universe. Proc Natl Acad Sci U S A 106:11079–11084. https://doi.org/10.1073/pnas.0905029106.
16. Godzik A. 2011. Metagenomics and the protein universe. Curr Opin Struct Biol 21:398–403. https://doi.org/10.1016/j.sbi.2011.03.010.
17. Dinsdale EA, Edwards RA, Hall D, Angly F, Breitbart M, Brulc JM, Furlan M, Desnues C, Haynes M, Li L, McDaniel L, Moran MA, Nelson KE, Nilsson C, Olson R, Paul J, Brito BR, Ruan Y, Swan BK, Stevens R, Valentine DL, Thurber RV, Wegley L, White BA, Rohwer F. 2008. Functional metagenomic profiling of nine biomes. Nature 452:629–632. https://doi.org/10.1038/nature06810.
18. Rondon MR, August PR, Bettermann AD, Brady SF, Grossman TH, Liles MR, Loiacono KA, Lynch BA, MacNeil IA, Minor C, Tiong CL, Gilman M, Osburne MS, Clardy J, Handelsman J, Goodman RM. 2000. Cloning the soil metagenome: a strategy for accessing the genetic and functional diversity of uncultured microorganisms. Appl Environ Microbiol 66:2541–2547. https://doi.org/10.1128/AEM.66.6.2541-2547.2000.
19. Simon C, Daniel R. 2011. Metagenomic analyses: past and future trends. Appl Environ Microbiol 77:1153–1161. https://doi.org/10.1128/AEM.02345-10.
20. Robertson DE, Chaplin JA, DeSantis G, Podar M, Madden M, Chi E, Richardson T, Milan A, Miller M, Weiner DP, Wong K, McQuaid J, Farwell B, Preston LA, Tan X, Snead MA, Keller M, Mathur E, Kretz PL, Burk MJ, Short JM. 2004. Exploring nitrilase sequence space for enantioselective catalysis. Appl Environ Microbiol 70:2429–2436. https://doi.org/10.1128/AEM.70.4.2429-2436.2004.
21. Lorenz P, Eck J. 2005. Metagenomics and industrial applications. Nat Rev Microbiol 3:510–516. https://doi.org/10.1038/nrmicro1161.
22. Bornscheuer UT. 2002. Microbial carboxyl esterases: classification, properties and application in biocatalysis. FEMS Microbiol Rev 26:73–81. https://doi.org/10.1111/j.1574-6976.2002.tb00599.x.
23. Martínez-Martínez M, Coscolín C, Santiago G, Chow J, Stogios PJ, Bargiela R, Gertler C, Navarro-Fernández J, Bollinger A, Thies S, Méndez-García C, Popovic A, Brown G, Chernikova TN, García-Moyano A, Bjerga GEK, Pérez-García P, Hai T, Del Pozo MV, Stokke R, Steen IH, Cui H, Xu X, Nocek BP, Alcaide M, Distaso M, Mesa V, Peláez AI, Sánchez J, Buchholz PCF, Pleiss J, Fernández-Guerra A, Glöckner FO, Golyshina OV, Yakimov MM, Savchenko A, Jaeger K-E, Yakunin AF, Streit WR, Golyshin PN, Guallar V, Ferrer M, The Inmare Consortium, The Inmare Consortium. 2018. Determinants and prediction of esterase substrate promiscuity patterns. ACS Chem Biol 13:225–234. https://doi.org/10.1021/acschembio.7b00996.
24. Arpigny JL, Jaeger KE. 1999. Bacterial lipolytic enzymes: classification and properties. Biochem J 343:177–183. https://doi.org/10.1042/bj3430177.
25. Lenfant N, Hotelier T, Velluet E, Bourne Y, Marchot P, Chatonnet A. 2013. ESTHER, the database of the alpha/beta-hydrolase fold superfamily of proteins: tools to explore diversity of functions. Nucleic Acids Res 41:D423–D429. https://doi.org/10.1093/nar/gks1154.
26. Littlechild JA. 2017. Improving the 'tool box' for robust industrial enzymes. J Ind Microbiol Biotechnol 44:711–720. https://doi.org/10.1007/s10295-017-1920-5.
27. Popovic A, Hai T, Tchigvintsev A, Hajighasemi M, Nocek B, Khusnutdinova AN, Brown G, Glinos J, Flick R, Skarina T, Chernikova TN, Yim V, Brüls T, Paslier DL, Yakimov MM, Joachimiak A, Ferrer M, Golyshina OV, Savchenko A, Golyshin PN, Yakunin AF. 2017. Activity screening of environmental metagenomic libraries reveals novel carboxylesterase families. Sci Rep 7:44103. https://doi.org/10.1038/srep44103.
28. Pellis A, Cantone S, Ebert C, Gardossi L. 2018. Evolving biocatalysis to meet bioeconomy challenges and opportunities. N Biotechnol 40:154–169. https://doi.org/10.1016/j.nbt.2017.07.005.
29. Antranikian G, Streit WR. 2022. Microorganisms harbor keys to a circular bioeconomy making them useful tools in fighting plastic pollution and rising CO2 levels. Extremophiles 26:10. https://doi.org/10.1007/s00792-022-01261-4.
30. Kruger A, Schafers C, Schroder C, Antranikian G. 2018. Towards a sustainable biobased industry: highlighting the impact of extremophiles. N Biotechnol 40:144–153. https://doi.org/10.1016/j.nbt.2017.05.002.
31. Atomi H. 2005. Recent progress towards the application of hyperthermophiles and their enzymes. Curr Opin Chem Biol 9:166–173. https://doi.org/10.1016/j.cbpa.2005.02.013.
32. Littlechild JA. 2015. Archaeal enzymes and applications in industrial biocatalysts. Archaea 2015:147671. https://doi.org/10.1155/2015/147671.
33. Vieille C, Zeikus GJ. 2001. Hyperthermophilic enzymes: sources, uses, and molecular mechanisms for thermostability. Microbiol Mol Biol Rev 65:1–43. https://doi.org/10.1128/MMBR.65.1.1-43.2001.
34. Alcaide M, Stogios PJ, Lafraya Á, Tchigvintsev A, Flick R, Bargiela R, Chernikova TN, Reva ON, Hai T, Leggewie CC, Katzke N, La Cono V, Matesanz R, Jebbar M, Jaeger KE, Yakimov MM, Yakunin AF, Golyshin PN, Golyshina OV, Savchenko A, Ferrer M, MAMBA Consortium. 2015. Pressure adaptation is linked to thermal adaptation in salt-saturated marine habitats. Environ Microbiol 17:332–345. https://doi.org/10.1111/1462-2920.12660.
35. Wei R, von Haugwitz G, Pfaff L, Mican J, Badenhorst CPS, Liu W, Weber G, Austin HP, Bednar D, Damborsky J, Bornscheuer UT. 2022. Mechanism-based design of efficient PET hydrolases. ACS Catal 12:3382–3396. https://doi.org/10.1021/acscatal.1c05856.
36. Heinl S, Hartinger D, Thamhesl M, Vekiru E, Krska R, Schatzmayr G, Moll WD, Grabherr R. 2010. Degradation of fumonisin B1, by the consecutive action of two bacterial enzymes. J Biotechnol 145:120–129. https://doi.org/10.1016/j.jbiotec.2009.11.004.
37. Rizzo C, Arcadi E, Calogero R, Sciutteri V, Consoli P, Esposito V, Canese S, Andaloro F, Romeo T. 2022. Ecological and biotechnological relevance of Mediterranean hydrothermal vent systems. Minerals 12:251. https://doi.org/10.3390/min12020251.

38. Zhou Z, Liu Y, Xu W, Pan J, Luo ZH, Li M. 2020. Genome- and community-level interaction insights into carbon utilization and element cycling functions of Hydrothermarchaeota in hydrothermal sediment. mSystems 5:e00795-19. https://doi.org/10.1128/mSystems.00795-19.
39. Park YJ, Yoon SJ, Lee HB. 2008. A novel thermostable arylesterase from the archaeon Sulfolobus solfataricus P1: purification, characterization, and expression. J Bacteriol 190:8086–8095. https://doi.org/10.1128/JB.00803-08.
40. Pereira MR, Maester TC, Mercaldi GF, de Macedo Lemos EG, Hyvonen M, Balan A. 2017. From a metagenomic source to a high-resolution structure of a novel alkaline esterase. Appl Microbiol Biotechnol 101:4935–4949. https://doi.org/10.1007/s00253-017-8226-4.
41. Coque JJ, Liras P, Martin JF. 1993. Genes for a beta-lactamase, a penicillin-binding protein and a transmembrane protein are clustered with the cephamycin biosynthetic genes in Nocardia lactamdurans. EMBO J 12:631–639. https://doi.org/10.1002/j.1460-2075.1993.tb05696.x.
42. Petersen EI, Valinger G, Solkner B, Stubenrauch G, Schwab H. 2001. A novel esterase from Burkholderia gladioli which shows high deacetylation activity on cephalosporins is related to beta-lactamases and DD-peptidases. J Biotechnol 89:11–25. https://doi.org/10.1016/s0168-1656(01)00284-x.
43. Placido A, Hai T, Ferrer M, Chernikova TN, Distaso M, Armstrong D, Yakunin AF, Toshchakov SV, Yakimov MM, Kublanov IV, Golyshina OV, Pesole G, Ceci LR, Golyshin PN. 2015. Diversity of hydrolases from hydrothermal vent sediments of the Levante Bay, Vulcano Island Aeolian archipelago identified by activity-based metagenomics and biochemical characterization of new esterases and an arabinopyranosidase. Appl Microbiol Biotechnol 99:10031–10046. https://doi.org/10.1007/s00253-015-6873-x.
44. Lewin A, Strand T, Haugen T, Klinkenberg G, Kotlar H, Valla S, Drablos F, Wentze A. 2016. Discovery and characterization of a thermostable esterase from an oil reservoir metagenome. Adv Enzyme Res 4:68–86. https://doi.org/10.4236/aer.2016.42008.
45. Leis B, Angelov A, Mientus M, Li H, Pham VT, Lauinger B, Bongen P, Pietruszka J, Goncalves LG, Santos H, Liebl W. 2015. Identification of novel esterase-active enzymes from hot environments by use of the host bacterium *Thermus thermophilus*. Front Microbiol 6:275. https://doi.org/10.3389/fmicb.2015.00275.
46. Miguel-Ruano V, Rivera I, Rajkovic J, Knapik K, Torrado A, Otero JM, Beneventi E, Becerra M, Sánchez-Costa M, Hidalgo A, Berenguer J, González-Siso MI, Cruces J, Rúa ML, Hermoso JA. 2021. Biochemical and structural characterization of a novel thermophilic esterase EstD11 provide catalytic insights for the HSL family. Comput Struct Biotechnol J 19:1214–1232. https://doi.org/10.1016/j.csbj.2021.01.047.
47. Sayer C, Szabo Z, Isupov MN, Ingham C, Littlechild JA. 2015. The structure of a novel thermophilic esterase from the Planctomycetes species, *Thermogutta terrifontis* reveals an open active site due to a minimal 'cap' domain. Front Microbiol 6:1294. https://doi.org/10.3389/fmicb.2015.01294.
48. Loi M, Fanell F, Liuzzi VC, Logrieco AF, Mule G. 2017. Mycotoxin biotransformation by native and commercial enzymes: present and future perspectives. Toxins (Basel) 9:111. https://doi.org/10.3390/toxins9040111.
49. Liu L, Xie M, We D. 2022. Biological detoxification of mycotoxins: current status and future advances. Int J Mol Sci 23:1064. https://doi.org/10.3390/ijms23031064.
50. Lyagin I, Efremenko E. 2019. Enzymes for detoxification of various mycotoxins: origins and mechanisms of catalytic action. Molecules 24:2362. https://doi.org/10.3390/molecules24132362.
51. McCormick SP, Price NP, Kurtzman CP. 2012. Glucosylation and other biotransformations of T-2 toxin by yeasts of the Trichomonascus clade. Appl Environ Microbiol 78:8694–8702. https://doi.org/10.1128/AEM.02391-12.
52. Hajighasemi M, Tchigvintsev A, Nocek B, Flick R, Popovic A, Hai T, Khusnutdinova AN, Brown G, Xu X, Cui H, Anstett J, Chernikova TN, Brüls T, Le Paslier D, Yakimov MM, Joachimiak A, Golyshina OV, Savchenko A, Golyshin PN, Edwards EA, Yakunin AF. 2018. Screening and characterization of novel polyesterases from environmental metagenomes with high hydrolytic activity against synthetic polyesters. Environ Sci Technol 52:12388–12401. https://doi.org/10.1021/acs.est.8b04252.
53. Tournier V, Topham CM, Gilles A, David B, Folgoas C, Moya-Leclair E, Kamionka E, Desrousseaux ML, Texier H, Gavalda S, Cot M, Guémard E, Dalibey M, Nomme J, Cioci G, Barbe S, Chateau M, André I, Duquesne S, Marty A. 2020. An engineered PET depolymerase to break down and recycle plastic bottles. Nature 580:216–219. https://doi.org/10.1038/s41586-020-2149-4.
54. Palm GJ, Fernández-Álvaro E, Bogdanović X, Bartsch S, Sczodrok J, Singh RK, Böttcher D, Atomi H, Bornscheuer UT, Hinrichs W. 2011. The crystal structure of an esterase from the hyperthermophilic microorganism Pyrobaculum calidifontis VA1 explains its enantioselectivity. Appl Microbiol Biotechnol 91:1061–1072. https://doi.org/10.1007/s00253-011-3337-9.
55. Sauvage E, Kerff F, Terrak M, Ayala JA, Charlier P. 2008. The penicillin-binding proteins: structure and role in peptidoglycan biosynthesis. FEMS Microbiol Rev 32:234–258. https://doi.org/10.1111/j.1574-6976.2008.00105.x.
56. Lee D, Das S, Dawson NL, Dobrijevic D, Ward J, Orengo C. 2016. Novel computational protocols for functionally classifying and characterising serine beta-lactamases. PLoS Comput Biol 12:e1004926. https://doi.org/10.1371/journal.pcbi.1004926.
57. Holm L. 2022. Dali server: structural unification of protein families. Nucleic Acids Res 50:W210–W215. https://doi.org/10.1093/nar/gkac387.
58. Wagner UG, Petersen EI, Schwab H, Kratky C. 2002. EstB from *Burkholderia gladioli*: a novel esterase with a beta-lactamase fold reveals steric factors to discriminate between esterolytic and beta-lactam cleaving activity. Protein Sci 11:467–478. https://doi.org/10.1110/ps.33002.
59. Delfosse V, Girard E, Birck C, Delmarcelle M, Delarue M, Poch O, Schultz O, Mayer C. 2009. Structure of the archaeal pab87 peptidase reveals a novel self-compartmentalizing protease family. PLoS One 4:e4712. https://doi.org/10.1371/journal.pone.0004712.
60. Flower DR, North AC, Sansom CE. 2000. The lipocalin protein family: structural and sequence overview. Biochim Biophys Acta 1482:9–24. https://doi.org/10.1016/s0167-4838(00)00148-5.
61. De Simone G, Galdiero S, Manco G, Lang D, Rossi M, Pedone C. 2000. A snapshot of a transition state analogue of a novel thermophilic esterase belonging to the subfamily of mammalian hormone-sensitive lipase. J Mol Biol 303:761–771. https://doi.org/10.1006/jmbi.2000.4195.
62. Kay BK, Williamson MP, Sudol M. 2000. The importance of being proline: the interaction of proline-rich motifs in signaling proteins with their cognate domains. FASEB J 14:231–241. https://doi.org/10.1096/fasebj.14.2.231.
63. Fadrosh DW, Ma B, Gajer P, Sengamalay N, Ott S, Brotman RM, Ravel J. 2014. An improved dual-indexing approach for multiplexed 16S rRNA gene sequencing on the Illumina MiSeq platform. Microbiome 2:6. https://doi.org/10.1186/2049-2618-2-6.
64. Distaso MA, Bargiela R, Brailsford FL, Williams GB, Wright S, Lunev EA, Toshchakov SV, Yakimov MM, Jones DL, Golyshin PN, Golyshina OV. 2020. High representation of archaea across all depths in oxic and low-pH sediment layers underlying an acidic stream. Front Microbiol 11:2871. https://doi.org/10.3389/fmicb.2020.576520.
65. R Core Team. 2020. R: a language and environment for statistical computing. R Foundation for Statistical Computing, Vienna, Austria.
66. Zhu W, Lomsadze A, Borodovsky M. 2010. Ab initio gene identification in metagenomic sequences. Nucleic Acids Res 38:e132. https://doi.org/10.1093/nar/gkq275.
67. Altschul SF, Madden TL, Schaffer AA, Zhang J, Zhang Z, Miller W, Lipman DJ. 1997. Gapped BLAST and PSI-BLAST: a new generation of protein database search programs. Nucleic Acids Res 25:3389–3402. https://doi.org/10.1093/nar/25.17.3389.
68. Edgar RC. 2004. MUSCLE: multiple sequence alignment with high accuracy and high throughput. Nucleic Acids Res 32:1792–1797. https://doi.org/10.1093/nar/gkh340.
69. Kumar S, Stecher G, Li M, Knyaz C, Tamura K. 2018. MEGA X: molecular evolutionary genetics analysis across computing platforms. Mol Biol Evol 35:1547–1549. https://doi.org/10.1093/molbev/msy096.
70. Tchigvintsev A, Tran H, Popovic A, Kovacic F, Brown G, Flick R, Hajighasemi M, Egorova O, Somody JC, Tchigvintsev D, Khusnutdinova A, Chernikova TN, Golyshina OV, Yakimov MM, Savchenko A, Golyshin PN, Jaeger KE, Yakunin AF. 2015. The environment shapes microbial enzymes: five cold-active and salt-resistant carboxylesterases from marine metagenomes. Appl Microbiol Biotechnol 99:2165–2178. https://doi.org/10.1007/s00253-014-6038-3.
71. Giunta CI, Cea-Rama I, Alonso S, Briand ML, Bargiela R, Coscolín C, Corvini PF-X, Ferrer M, Sanz-Aparicio J, Shahgaldian P. 2020. Tuning the properties of natural promiscuous enzymes by engineering their nano-environment. ACS Nano 14:17652–17664. https://doi.org/10.1021/acsnano.0c08716.
72. Minor W, Cymborowski M, Otwinowski Z, Chruszcz M. 2006. HKL-3000: the integration of data reduction and structure solution–from diffraction images to an initial model in minutes. Acta Crystallogr D Biol Crystallogr 62:859–866. https://doi.org/10.1107/S0907444906019949.
73. Liebschner D, Afonine PV, Baker ML, Bunkóczi G, Chen VB, Croll TI, Hintze B, Hung LW, Jain S, McCoy AJ, Moriarty NW, Oeffner RD, Poon BK, Prisant MG, Read RJ, Richardson JS, Richardson DC, Sammito MD, Sobolev OV, Stockwell DH, Terwilliger TC, Urzhumtsev AG, Videau LL, Williams CJ, Adams PD. 2019. Macromolecular structure determination using X-rays, neutrons and electrons: recent developments in Phenix.

Acta Crystallogr D Struct Biol 75:861–877. https://doi.org/10.1107/S2059798319011471.
74. Jumper J, Evans R, Pritzel A, Green T, Figurnov M, Ronneberger O, Tunyasuvunakool K, Bates R, Žídek A, Potapenko A, Bridgland A, Meyer C, Kohl SAA, Ballard AJ, Cowie A, Romera-Paredes B, Nikolov S, Jain R, Adler J, Back T, Petersen S, Reiman D, Clancy E, Zielinski M, Steinegger M, Pacholska M, Berghammer T, Bodenstein S, Silver D, Vinyals O, Senior AW, Kavukcuoglu K, Kohli P, Hassabis D. 2021. Highly accurate protein structure prediction with AlphaFold. Nature 596:583–589. https://doi.org/10.1038/s41586-021-03819-2.
75. Emsley P, Cowtan K. 2004. Coot: model-building tools for molecular graphics. Acta Crystallogr D Biol Crystallogr 60:2126–2132. https://doi.org/10.1107/S0907444904019158.